GULF RADIATION TECHNOLOGY

Gulf-RT-10642

RADIATION-INDUCED CONDUCTIVITY IN MISSILE SITE MATERIALS

FINAL REPORT ON TASK 5-4

by

T. M. Flanagan and R. A. Cesena

TN 122

Prepared for
Air Force Special Weapons Center
Kirtland AFB, New Mexico

under
Contract F29601-70-C-0029
Gulf Rad Tech Project 6135

May 7, 1971

GULF RADIATION TECHNOLOGY
A DIVISION OF GULF ENERGY & ENVIRONMENTAL SYSTEMS COMPANY
P.O. BOX 608, SAN DIEGO, CALIFORNIA 92112

ACKNOWLEDGEMENTS

The authors would like to acknowledge the very helpful discussions with Dr. Giovanni Caprioglio, Gulf General Atomic, Mr. Robert Bigelow, and Mr. Rod Carroll of the U.S.G.S., Mr. Rick Schaeffer, Rand Corp., and Captain Larry West, USAF, the contract monitor.

1. INTRODUCTION

When energetic radiation passes through matter, Compton and photoelectric interactions with atomic electrons produce electron-ion pairs. The electron then loses energy through scattering processes, creating other free electrons and vibrational excitations until the electrons are thermalized. These processes occur within about 10^{-12} sec of the initial interaction. The ions and electrons are then subject to diffusion, drift in an external applied field, and trapping until recombination returns the material to its preirradiation state. Recombination times can be as fast as the thermalization time to as long as seconds, depending on the microscopic structure of the material.

During the time the charge carriers are free to move, they contribute to the conductivity of the material, producing a radiation-induced conductivity (RIC) component. The magnitude of the RIC depends on the radiation, the temperature, and the mobilities and lifetimes of the liberated carriers. Since the latter two quantities depend on the atomic structure of the material in question, RIC is not, in general, predictable a priori and must be determined experimentally.

The magnitude of the RIC induced in structures and in the ground around missile sites must be known in order to calculate the magnitude of the EMP expected from a given radiation environment. To assist in the evaluation of the EMP threat to existing and future sites, a program of research was initiated into the RIC of typical site construction materials.

The program is divided into two parts. In the first part, the RIC in a sampling of concrete material is examined to scope the magnitude of the enhancement in site structures. The second portion of the program deals with the earth and fill materials at the site. Since studies of the RIC in these materials pose special experimental problems, during this

program the effort was directed toward defining methods for handling and measuring samples of these materials in such a way that the results could be related to in situ materials. This report describes the results of these efforts.

2. MODEL OF THE RADIATION-INDUCED CONDUCTIVITY

Concrete is a difficult material to model because of its lack of homogeneity. Large chunks of aggregate are mixed with sand, cement, and air voids, all of which can be expected to have different RIC characteristics and temperature dependences. In addition, the large number of interfaces at which charge can be accumulated makes a complete modeling of the conduction processes in concrete a formidable task.

However, if we only ask for empirical relationships which give some qualitative description of the conduction processes, the task is more reasonable. The models developed for pure insulators can then be applied as though concrete were a homogeneous substance, while always remembering that the conclusions which depend on detailed structure must be modified in the light of the real structure of concrete.

2.1 AMBIENT CONDUCTIVITY

The conductivity of a material in the absence of external radiation is called the ambient conductivity and can be described by

$$\sigma = e \sum_i \mu_i N_i z_i \quad , \tag{1}$$

where e = electronic charge,
μ_i = mobility of the i^{th} carrier type,
N_i = density of the i^{th} carrier type,
z_i = ionization number of the i^{th} carrier type.

In the absence of external generation, the number of free electrons is negligible, and the conduction is ionic. Thus, the ambient conductivity can be expected to measure the effective μNz product for the material.

2.2 RADIATION-INDUCED CONDUCTIVITY

The radiation-induced conductivity is given by a similar expression

$$\sigma = e \left(\sum_j \mu_j N_j + \mu_e n_e \right) , \qquad (2)$$

where the symbols for ions are the same as in Eq. 1, except these are now radiation-produced ions, and

μ_e = electronic mobility,
n_e = free electron density.

The quantities μ_e and n_e are averages over the concrete, since they will be different in the various materials which make up the concrete.

The mobility can be written

$$\mu = \frac{e}{m} \langle \tau_r \rangle , \qquad (3)$$

where m is the mass of the carriers and $\langle \tau_r \rangle$ is an effective scattering relaxation time.

Since m for ionic conduction is much larger than m for electrons, the ionic mobility is much less than that for electrons. However, due to the possibility of rapid formation of negative ions in solution, the ionic conductivity cannot be neglected a priori.

It is useful at this point to anticipate the results somewhat. Referring to Fig. 26 in Section 5, a representative value of the conductivity at 10^9 rad/sec is 10^{-8} $(\text{ohm-cm})^{-1}$. We would like to estimate the effective mobility of the dominant carriers. In steady state, the conductivity can be described by[1]

$$\sigma = g \tau_e e\mu , \qquad (4)$$

where g = generation rate of carriers and
τ_e = effective lifetime of the carriers.

The generation rate is related to the dose rate through

$$g = 6.25 \times 10^{14} \frac{\rho \dot{\gamma}}{E_p} \text{ (cm}^3\text{-sec)}^{-1} , \qquad (5)$$

where ρ = density in g/cm^3,

$\dot{\gamma}$ = dose rate in rad/sec,

E_p = energy (in eV) required to produce an electron-ion pair.

Using a reasonable value (~100 eV) for E_p, $g \approx 10^{21}$ (cm^3-sec)$^{-1}$ at 10^9 rad/sec. From our data, we know $\tau_e \leq 10^{-9}$ sec, then

$$\mu = \frac{\sigma}{g \tau_e e} = \frac{10^{-9}}{(10^{21})(10^{-9})(1.6 \times 10^{-19})} \approx 10^{-1} \text{ cm}^2/\text{volt-sec.}$$

This number is probably on the small side, since the lifetime is probably shorter than 10^{-9} sec and E_p may be greater than 100 eV. Since the mobility of ions is of the order of 10^{-3}, we conclude that the RIC is dominated by electronic motion.

This anticipation of the results is useful, since it allows discussion of the RIC in terms of electronic models. As mentioned earlier, all of the pertinent lifetimes are much shorter than the radiation pulse widths. Hence, there will be a steady-state condition with respect to generation and recombination, and a steady-state model is appropriate.

Considering the real material, some quasi-energy gap is expected since, as mentioned above, very short lifetime mobile states are observed when electrons are excited by radiation. From radiation chemistry data[2] and insulator data,[3] we expect rapid capture of electrons in mobile states by centers which have levels above the equilibrium energy levels (ions, trapping, and recombination states). Considering the disorder and composite character of concrete, these levels are expected to be distributed in energy below the free states.

A useful model for discussing the phenomena is one developed by Rose,[4] and to develop this model, let us shift our thinking to an idealized insulation with a conduction band (free states) and valence band (ion states) with

distributed trapping and recombination centers in the forbidden gap. Let the states be distributed in an exponentially decreasing density below the conduction band as

$$N_t(E) = A \exp [-(E_c - E_t)/kT_1)] \quad . \tag{6}$$

The temperature T_1 is a formal parameter that can be adjusted to make the density of trapping states vary more or less rapidly with energy.

Without going into the details of the kinetic equations, since such a discussion is not particularly germane to a discussion of concrete, it can be seen that such a model predicts a sublinear dependence of the free-carrier concentration on dose rate. At very low dose rates, the equilibrium populations of the trapping and recombination centers are not significantly perturbed. As the dose rate is increased, the lower-lying trapping levels are filled and thereby converted to recombination centers. The increase in the relative density of recombination centers with increasing dose rate causes the lifetime of the carriers to decrease with increasing dose rate. From Eq. 4, it can be seen that the conductivity is directly proportional to a product of the dose rate (generation rate) and the lifetime. Thus, the increasing dose rate and decreasing lifetime produce a sublinear conductivity variation.

Rose[4] shows that the carrier concentration varies as

$$n \propto g^{(T_1/T_1+T)} \quad . \tag{7}$$

Depending on the value of T_1, the conductivity is proportional to the dose rate raised to a power between 0.5 and 1.0.

Note that this assumes that the mobility is not a function of the dose rate. There are two mechanisms whereby the dose rate may affect the mobility. The first is an increase in the carrier scattering. The second is a change in the barriers between components of the concrete due to ionization-induced potential barrier changes. A discussion of these points requires an examination of the experimental data, and this point is taken up in Section 5.

3. CONCRETE SAMPLES

3.1 SAMPLE SELECTION

Eighteen plugs of concrete, representing various structures on Site I-6, were obtained through the Air Force Weapons Laboratory. The plugs were about 2.25 in. in diameter and approximately 2 in. long. A map indicating the locations from which the cores were taken is shown in Fig. 1.

The parameters which are expected to be of importance for the conductivity in concrete are the size and type of inhomogeneities, density, porosity, water content, and composition. These vary greatly by virtue of the origin of the core plug. Plugs taken from flat, horizontal, accessible areas tend to be more porous, have fewer inhomogeneities, and are less dense than those taken from walls where, perhaps, the pour cannot be easily tamped or settled. Also, the inner ends of the plugs tend towards aggregate and larger ratios of aggregate to cement-sand, for the same reason. The samples selected thus show considerable variation in the composition and inhomogeneities, and can be regarded as a representative sampling.

3.2 SAMPLE SIZE

A sample large enough to contain a representative composition of voids, cement-sand, and aggregate is desirable to represent the concrete in a structure. Since the aggregate is the largest inhomogeneity in the concrete, a sample which is larger than the average aggregate size should be chosen. On the other hand, the irradiation beam must uniformly cover the sample, and the thickness of the sample should not be so large that the energy deposition is nonuniform.

It was found that a large number of inhomogeneities would be included within a 2.5-cm diameter, while fairly high dose rates could still be maintained uniformly across such an area. Thus, 2.5 cm was chosen as the measuring electrode diameters.

Since 30-MeV electrons were to be used as the ionization source, the thickness of the sample should be such that (1) the energy is not degraded

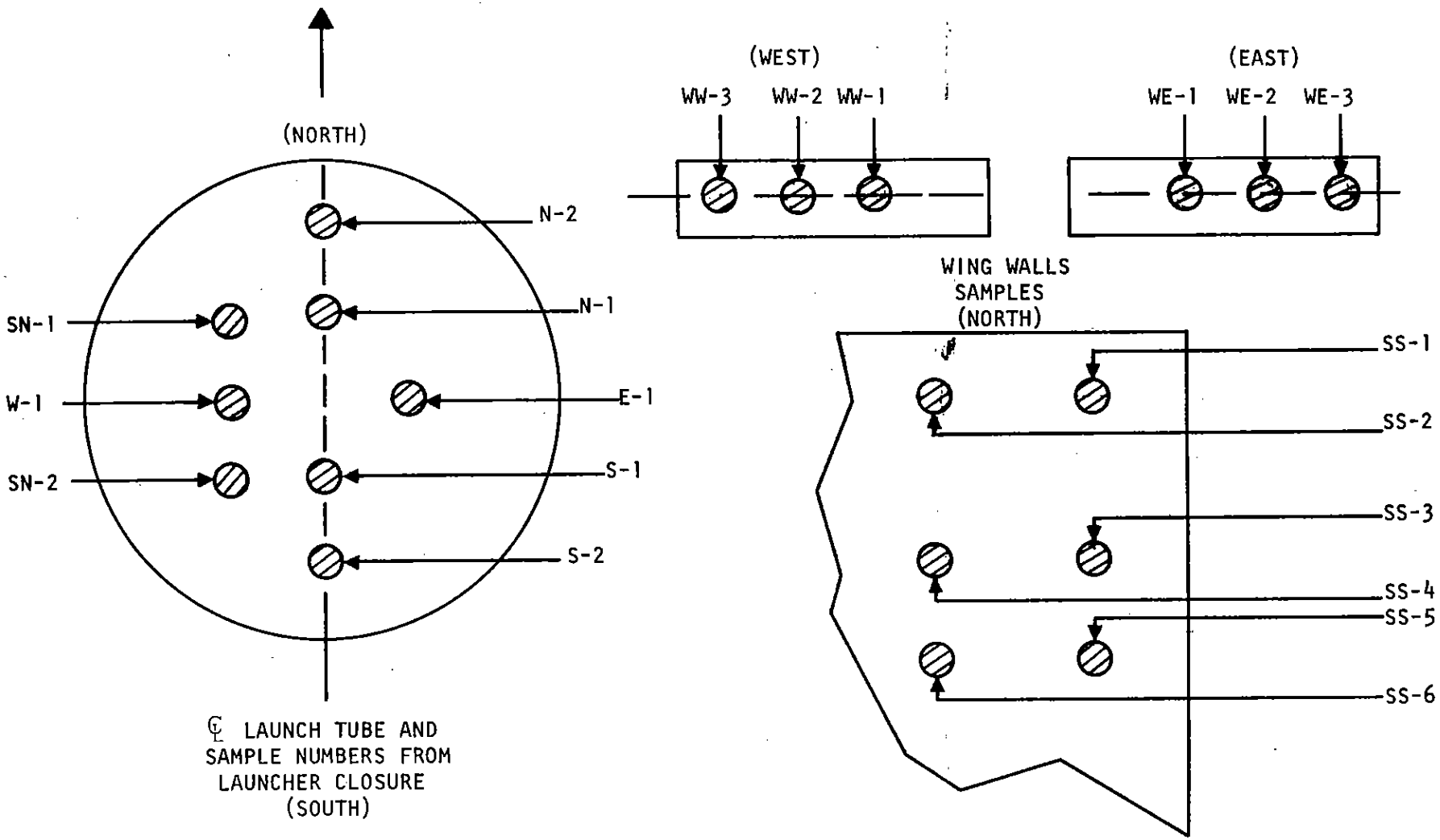

Fig. 1 Schematic of launch facility showing relative origins of concrete samples

sufficiently to cause nonuniform energy deposition and (2) the beam is not spread significantly by scattering. Since the range of a 30-MeV electron is about 7 cm in concrete (average density 2 g/cm^3), the second consideration is overriding. It was found that a total sample thickness of about 1 cm could be tolerated without serious beam spreading, and this dimension was fixed as the total sample thickness.

3.3 SAMPLE PREPARATION

A total of eighteen concrete samples, taken from various locations at the site and properly identified, were received in the form of cylinders with an average diameter of 2-1/4 in. (5.7 cm) and an average length of 2 in. (5.2 cm). Five representative samples were selected from the assortment, based on their locations at the site and their suitability from the standpoint of length and quality. These were center-ground using a diamond dressing wheel to an outside diameter of 2.000 in.; each was then sliced into as many 0.200-in. thick discs as possible. Tolerances of ±0.001 in. were placed on these dimensions, but were difficult to hold in the parting phase. A final lapping using carborundum paper was required to ensure a flat surface.

All samples were coded on their edges with the plug identification number and with a number representing their position in the plug.

The samples were carefully examined, and pairs from each plug were selected. The selected pairs were vacuum dried, and then each disc was weighed, and its dimensions were measured and recorded.

Silver contacts were then deposited on each sample by vacuum-evaporation techniques. The total mass of metal deposited on the samples was less than a milligram. The front and back electrode design, shown in Fig. 2, is based on standard conductivity techniques employed in this laboratory.[5]

Following deposition of electrodes, the moisture content of the samples was adjusted. To saturate a sample with water, the sample is placed in a vacuum (~10^{-3} torr) for 1 to 2 days. Then the sample is immersed in water without breaking the vacuum. Air is then admitted, forcing the water into the sample under atmospheric pressure. Samples prepared in this way are

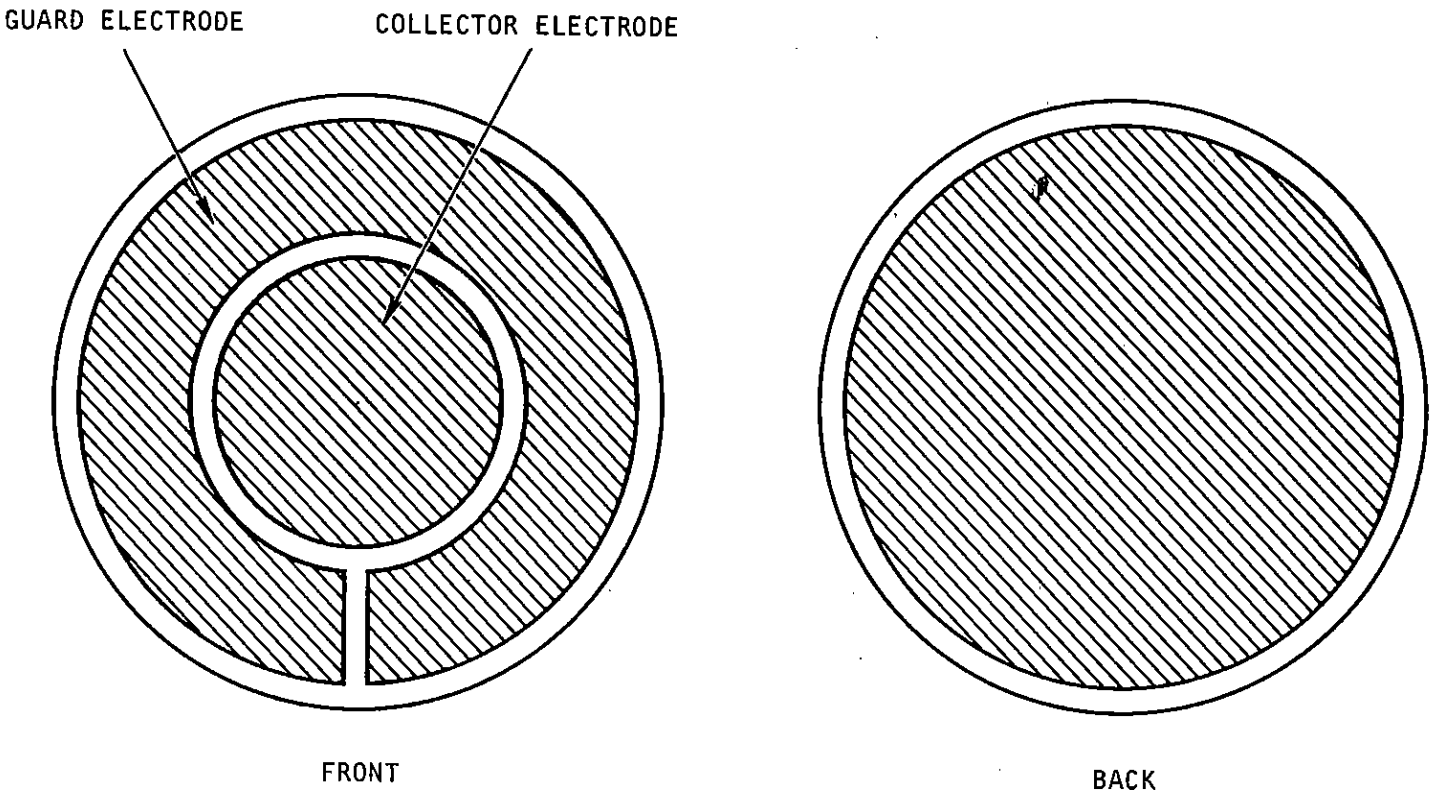

Fig. 2 Schematic showing the electrode design obtained by vacuum-evaporating silver through a mask. Two concrete samples are sealed front-to-front in the sample holder.

referred to as "wet" samples in this report, and they contain 5 to 9% water by weight. The samples referred to in this report as "dry" or "ambient" are in equilibrium with the ambient humidity (~45% relative humidity at ~20° C) and contain between 0.9 to 2.1% water by weight. A sample which was vacuum-dried was also measured; its water content was less than 0.01% by weight, and is referred to as a "very dry" sample.

After the sample water content was adjusted, the samples were weighed and sealed into the test chamber.

3.4 SAMPLE HOLDER

To preclude shunt currents resulting from air ionization, which can be quite large and long-lived, a special sample holder was designed and built which hermetically encapsulated the samples and itself fit into a larger vacuum chamber. A surrounding vacuum was required to bring out the electrical leads through the high-radiation region, and to provide thermal isolation which permits the low-temperature work and facilitates the control of the desired temperature. Figure 3 shows a cross section of the holder which is basically two heavy flanges of 6061-T6 aluminum designed to take the severe sample expansion forces occurring at high temperatures without permanent distortion. The front flange is machined to 0.030 in. over the effective sample area to prevent excessive beam energy degradation. The back flange contains two 150-watt cartridge heater elements for heating and also has a chamber in which a refrigerant is circulated when needed. By the use of two guide pins, the two flanges assemble coaxially within 0.001 in.

The liner which immediately surrounds each sample is a cup machined out of polyethylene to fit the sample—a result of the difficulty in parting and lapping each disc to the required tolerances. This cup provides the necessary electrical insulation and cushioning and also provides a primary seal which locks in the sample water during the initial assembly. After a satisfactory initial assembly and electrical checkout, a low-viscosity nonadhering silicone epoxy is injected under high pressure into a channel or ring formed by the beveled edges of each cavity and polyethylene cup. After polymerizing, the silicone forms an effective O-ring

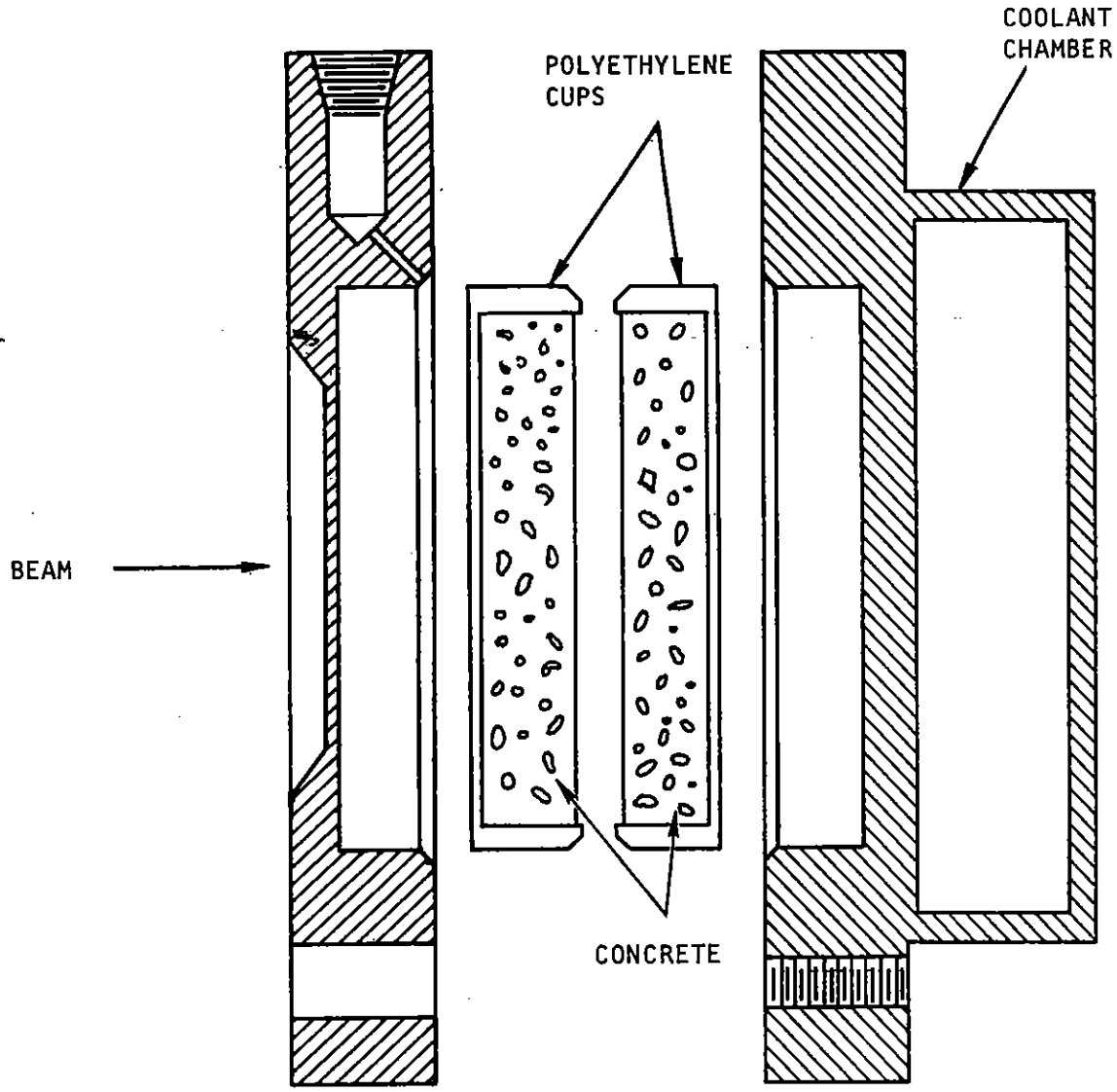

Fig. 3. Sectional view of sample holder used to hermetically contain concrete samples. Heaters, thermocouples, and electrical connections are not shown.

seal around the polyethylene liner and around the small-gage electrical leads and thermocouples attached to the samples. This holder has been found to be suitable for the temperatures used for testing concrete in this program, i.e., -50°C to +100°C.

Required electrical connections into the chamber are: one applied voltage lead connecting, internally, the two outside faces of the paired sample; one guard-ring lead from an outside ground; a collector lead; two copper-constantan (No. 36) thermocouples. Figure 4 shows the two samples and their respective electrode systems and the internal connections; the leads are 0.005-in.-dia. silver wires. Each lead, which is insulated with Teflon spaghetti, is brought in through holes drilled in radially, parallel to the plane of the inner faces of the sample holder. Since the sample temperature changes lag the flange temperature changes due to the poor thermal conductivity of the polyethylene liner, a third thermocouple monitors the flange temperature and is used to drive the temperature controller. Temperature equilibrium is achieved when the flange and sample thermocouples indicate the same temperature.

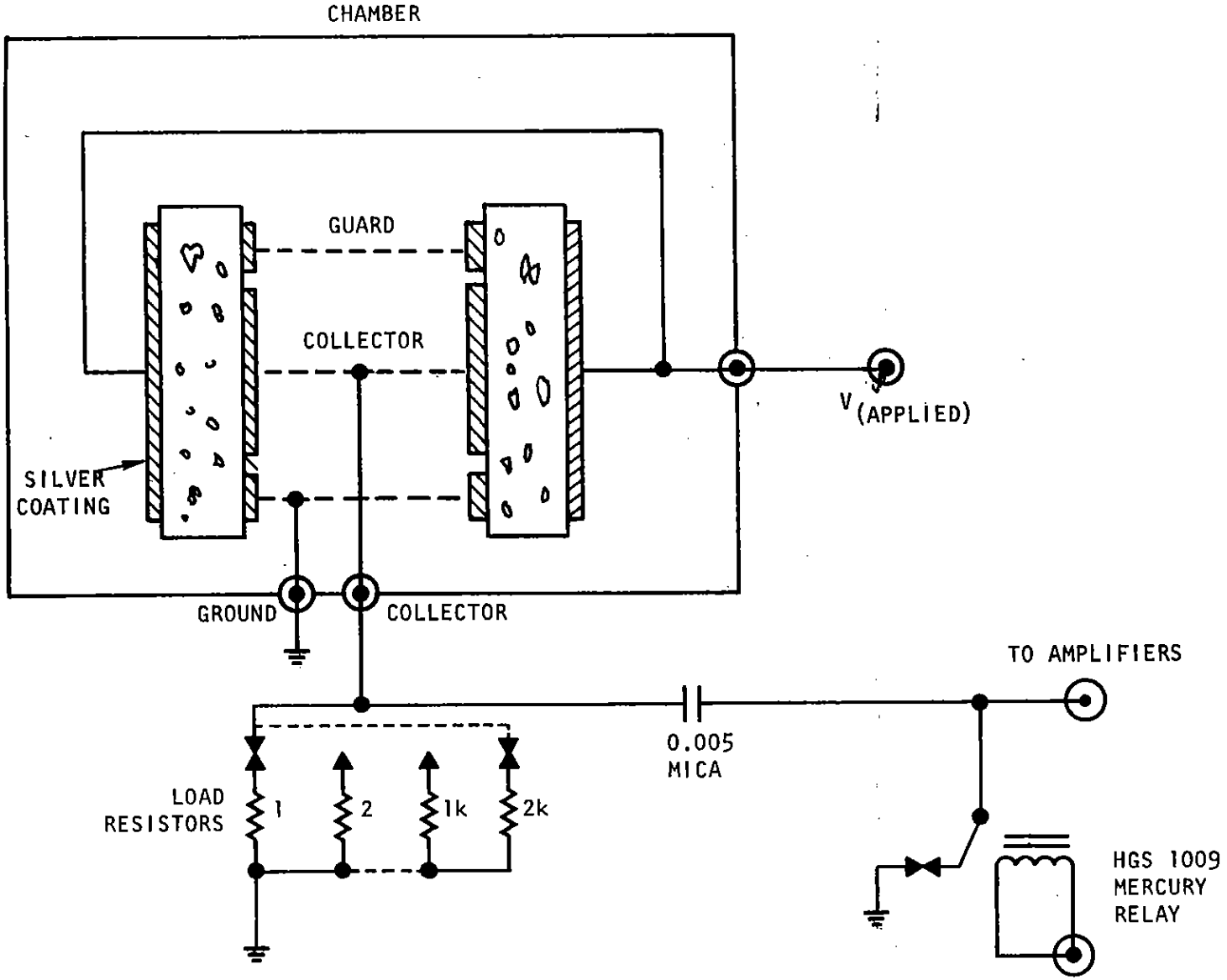

Fig. 4 Schematic of the electrical connections made to the concrete samples. The collector potential is held to less than a volt by remote selection of a suitable load resistor. The mercury relay is normally closed.

4. AMBIENT CONDUCTIVITY IN CONCRETE

4.1 MEASURING TECHNIQUE

The ambient conductivity is the value of the electrical conductivity measured without irradiation. Figure 5 is a schematic of the necessary equipment for the ambient conductivity measurements. The voltage is applied with a pulsed voltage source, and the current is monitored with an external variable-load resistor. The load resistor is adjusted so that, at most, a few percent of the value of the applied voltage is dropped across this resistor. The voltage applied to the sample and the voltage across the load resistor corresponding to the current flowing through the sample are displayed on the oscilloscope, and photographed. Because a pulsed voltage source is used in making the conductivity measurements, a charging transient is seen at the beginning of the current signal. This transient arises from the effects of lead and electrode capacitance and from polarization within the sample, and exhibits two or more time constants. The influence of these effects on the computed conductivity is reduced by extrapolating the current signal back to t = 0 from ~5-10 lifetimes later (10-20 μsec). The error in the conductivity is estimated to be less than 5%. (See Appendix 1 for discussion of polarization and other electrode effects.) The conductivity is then computed from

$$\sigma = \frac{I}{V_0} \frac{\ell}{2A} \quad ,$$

where

V_0 = applied voltage (volts),
I = current through sample (amps),
ℓ = single sample thickness (cm),
A = area of center electrode (cm^2).

The factor of 2 arises from the double sample arrangement.

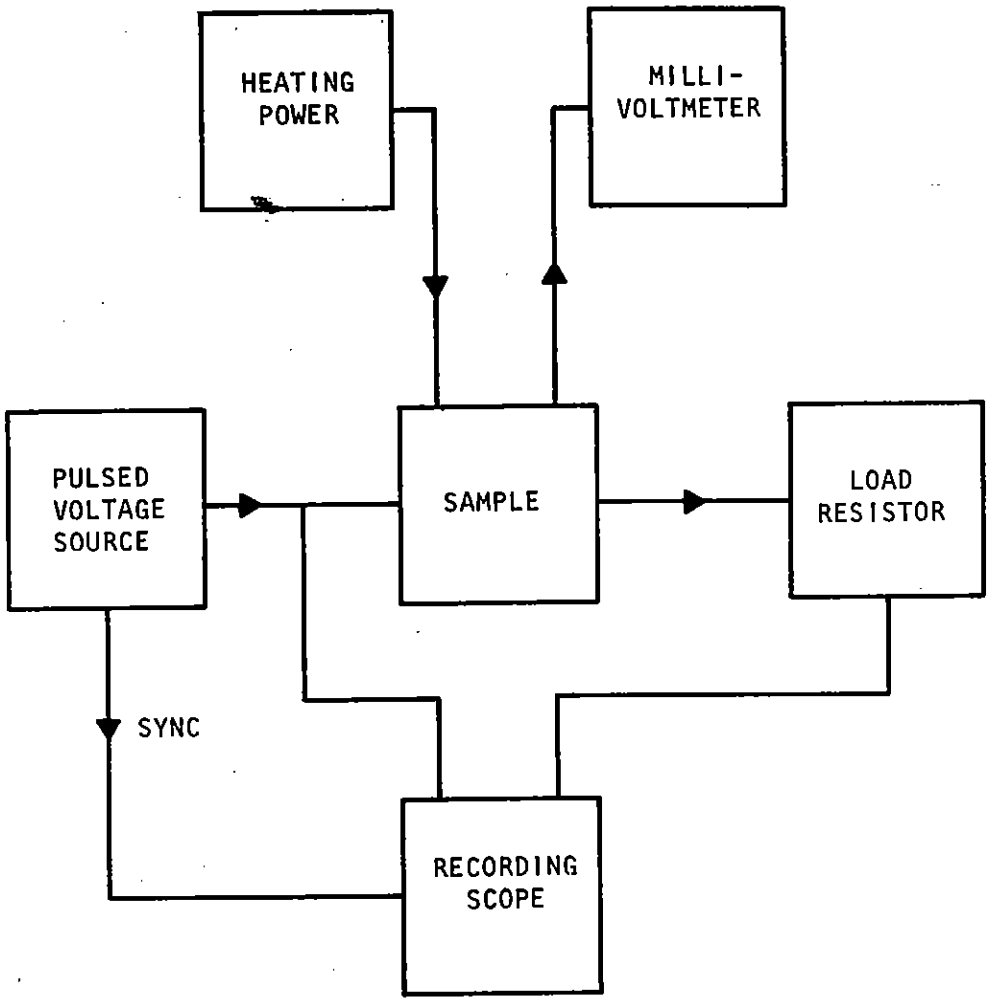

Fig. 5 Schematic of the experimental setup to measure the ambient conductivity in concrete

4.2 AMBIENT CONDUCTIVITY RESULTS

To measure the ambient conductivity, a saturated sample (WW-2) was suspended on a weighing pan in a low-humidity chamber. The moisture was removed by very slow diffusion and evaporation so that the sample had a negligible internal moisture gradient. The conductivity and weight of the sample were monitored as the sample dried out. Figure 6 shows the ambient conductivity at 20° C versus water content.

As a check on the results, the sample was again raised to ambient water content (1.2%) and allowed to come to equilibrium. The ambient conductivity was measured to be $\sim 1.5 \times 10^{-6}$ $(\text{ohm-cm})^{-1}$, which is in good agreement with the slow-drying experiment.

The ambient conductivity from -50° C to ~100° C for sample WW-2, with a 1.2% water content, is shown in Fig. 7. The conductivity is plotted versus 1000/T to facilitate the computation of the activation energy. The conductivity is given by

$$\sigma = 11.5 \exp(-0.40/kT) \quad .$$

Figure 8 shows the ambient conductivity versus 1000/T for a very dry sample, WE-2. The equation of the conductivity curve is

$$\sigma = 0.15 \exp(-0.34/kT) \quad .$$

The activation energies are reasonably similar in both cases, indicating that the conductivity processes are common for a very dry sample and for an ambient moisture sample. The factor of ~100 higher σ_0 for the wetter sample reflects the higher ionic concentration of the pore water.

Figure 9 shows the ambient conductivity of two wet samples. For one sample, a set of platinum-Ag:AgCl blotter electrodes, obtained through the courtesy of the U.S. Geological Survey, was used, while for the other, silver contacts were evaporated on the sample in the manner described previously. The two electrode types give similar conductivity behavior within the deviations expected for two different samples. The conductivity is seen to rise steeply with temperature below 0° C ($10^3/T = 3.66°K^{-1}$), with an activation energy of about 2 eV, while above 0° C, the activation energy is

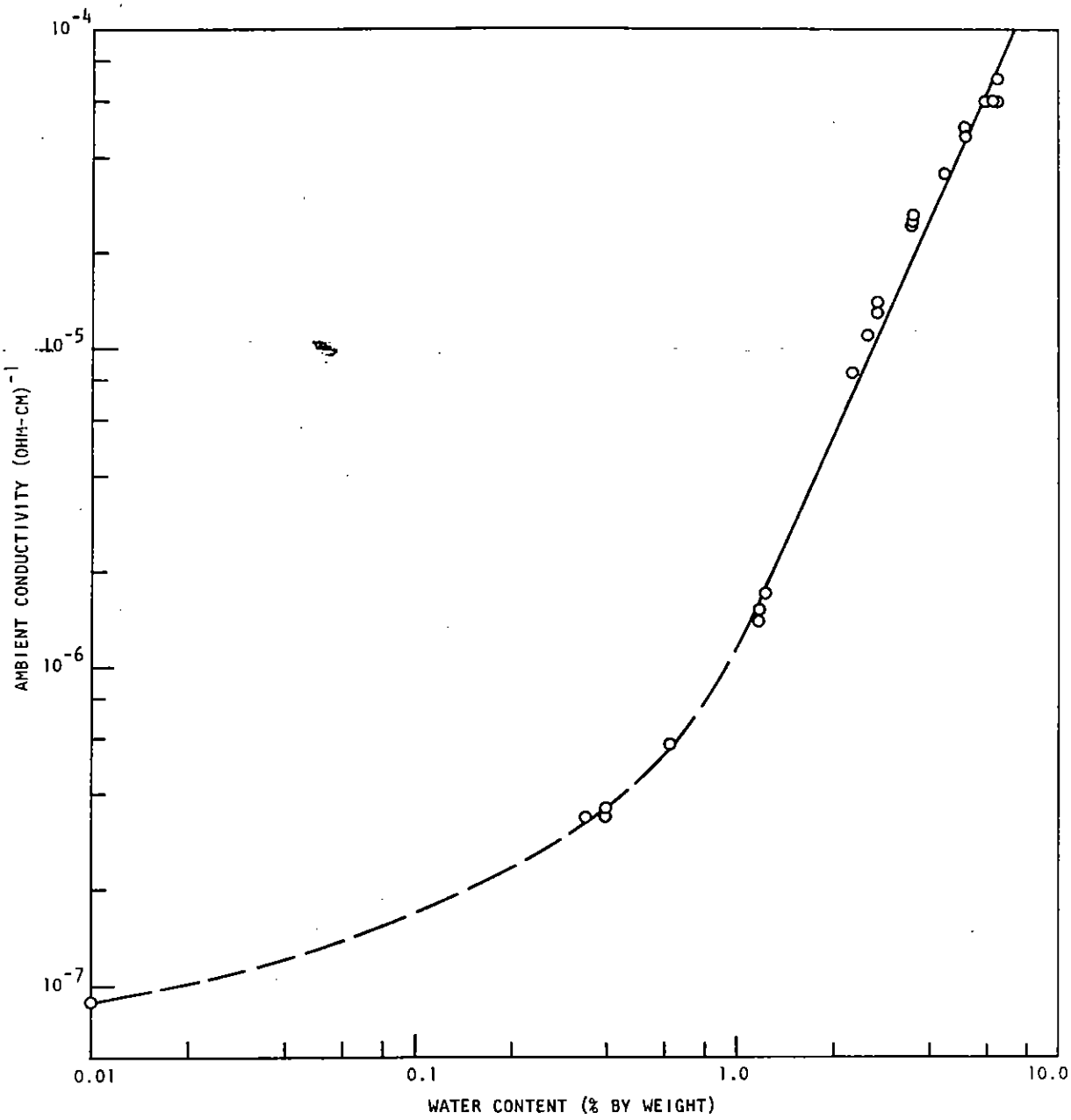

Fig. 6 Ambient conductivity as a function of water content of sample (WW-2) at 19-21°C

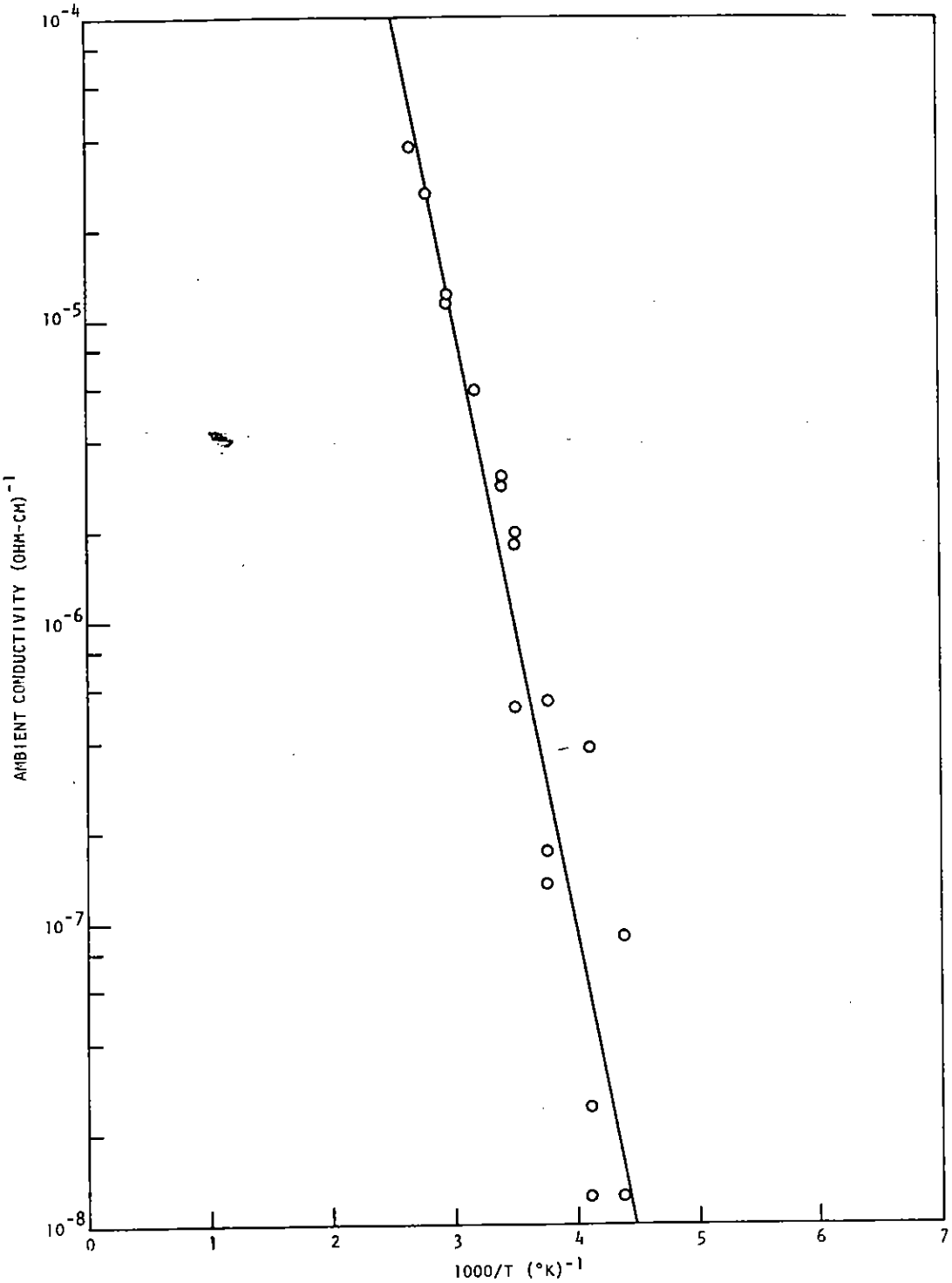

Fig. 7 Ambient conductivity as a function of reciprocal temperature for sample (WW-2-1,WW-2-2); moisture content 1.2% by weight. The conductivity is given by $\sigma = 11.5 \exp(-0.40/kT)$.

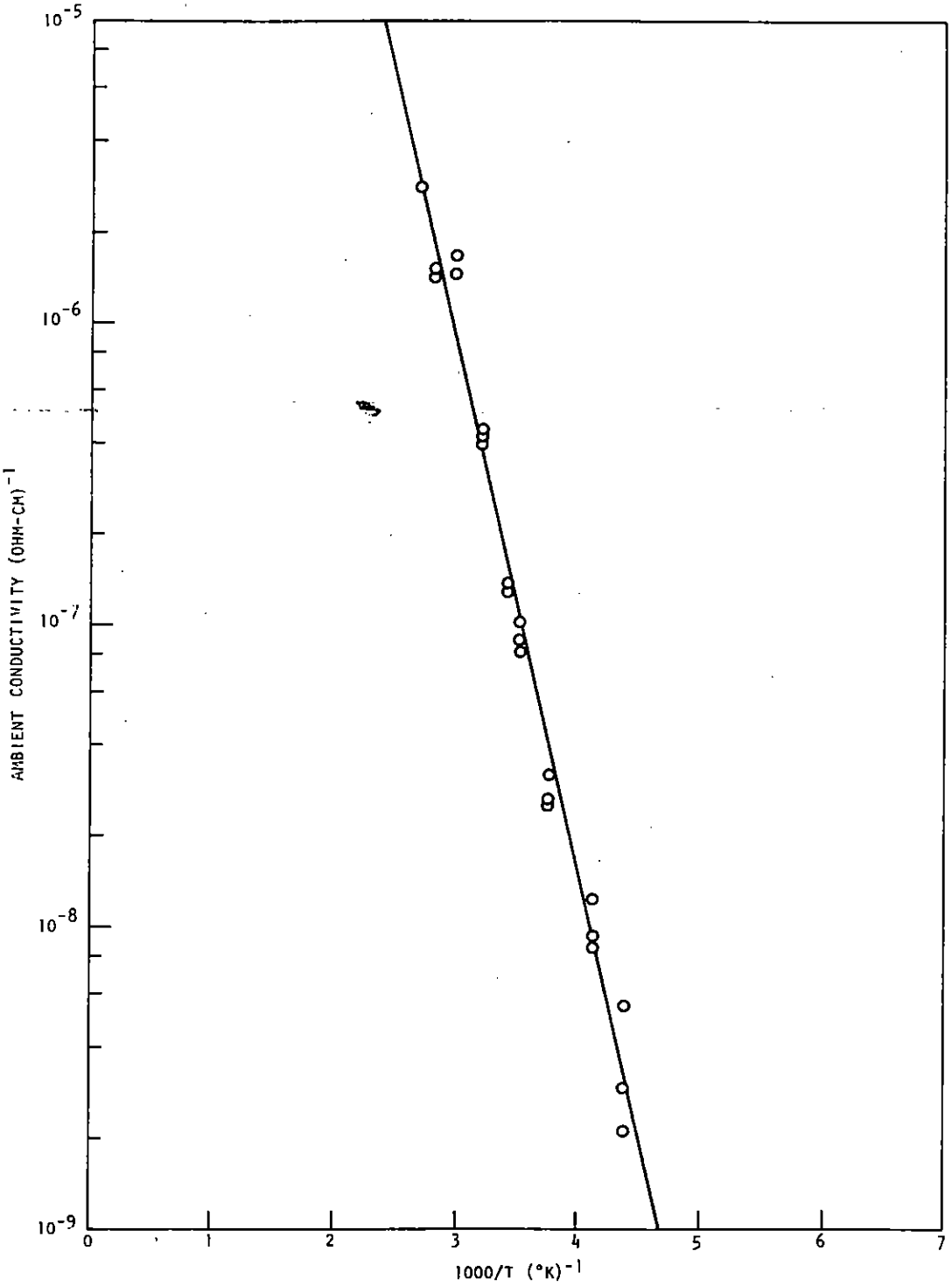

Fig. 8 Ambient conductivity as a function of reciprocal temperature for very dry sample (WE-2-1, WE-2-2). The conductivity is given by $\sigma = 0.15 \exp(-0.34/kT)$.

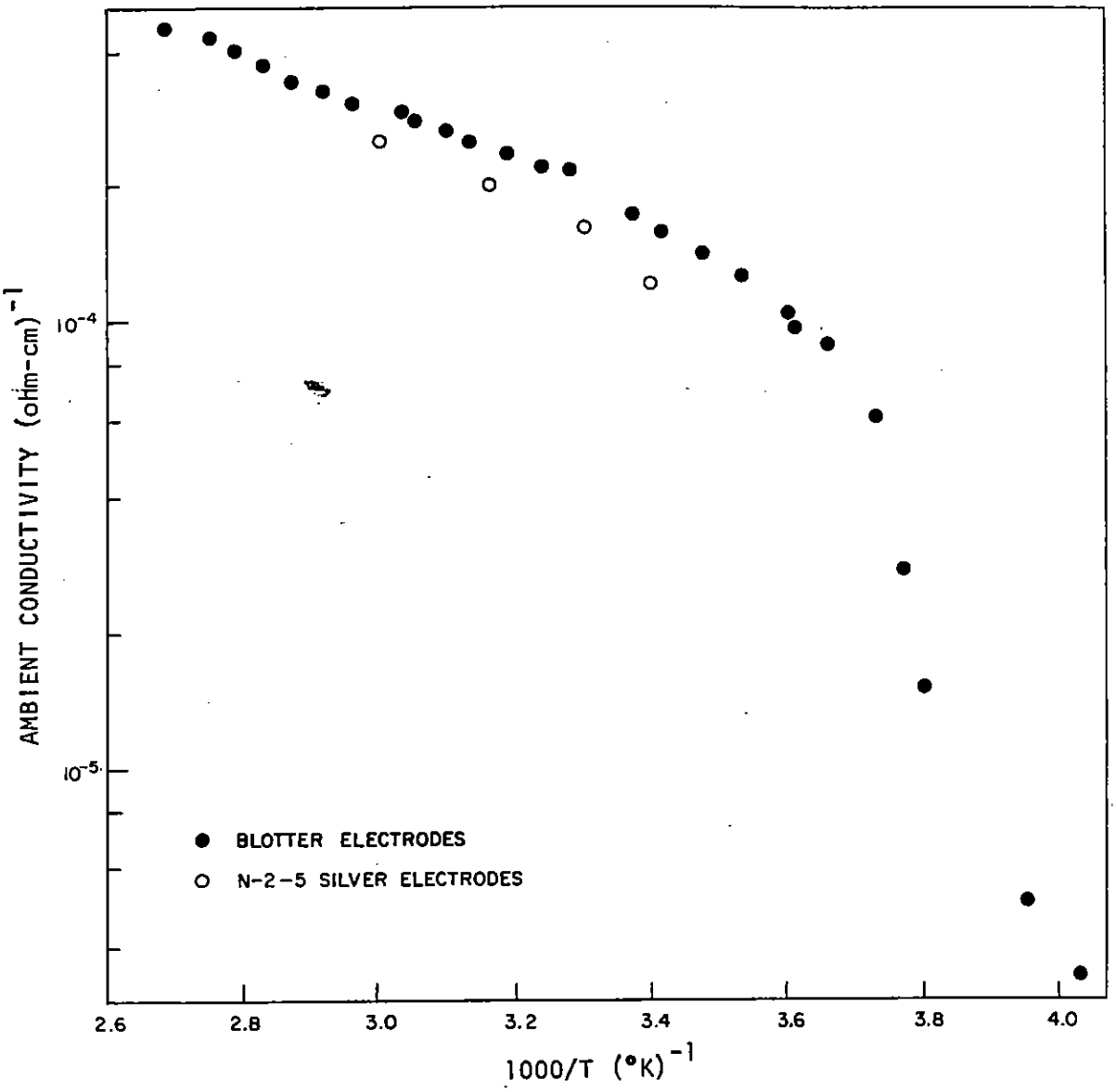

Fig. 9 Ambient conductivity of wet sample as a function of reciprocal temperature

about 0.2 eV. The absence of a jump in the conductivity at 0°C, indicates that both the ion mobility and the ion concentration are increasing steadily as the sample is warmed toward 0°C. These quantities continue to increase above 0°C, but at a slower rate, due both to increased ion mobility and to increase in the solubility of ionic species.

4.3 TRANSIENT RADIATION-INDUCED CONDUCTIVITY IN CONCRETE

4.3.1 Experimental

The transient conductivity measurements were carried out using pulses of 30-MeV electrons for ionization, from the Gulf Radiation Technology linear accelerator (Linac). With this machine, dose rates to 10^{10} rad/sec were obtainable over the sample area, and pulse widths from 10 nsec to 4.5 μsec are available. A secondary-emission beam monitor was used to measure the relative dose per Linac pulse, and was calibrated against a thermistor calorimeter placed at the sample position. Signals were brought out in coaxial cables and monitored with radiation-hardened amplifiers. The Linac instrumentation consists of two differential amplifiers with a gain of 40 db and rise time of 25 nsec, which differentially drive an oscilloscope. Remote attenuation is possible so that deflection sensitivities between 50 μV/cm and 4 V/cm are possible at the oscilloscope. The oscilloscope is a dual-beam device; for each Linac pulse, a photograph of the sample signal and of the secondary emission beam monitor signal can be taken. With this system, time-resolved *in situ* measurements of the radiation-induced conductivity are performed.

The instrumentation for measuring the transient conductivity is the same as that for the ambient conductivity with some additions (1) to achieve proper timing for the voltage and Linac pulses and (2) to enhance the sensitivity of the system to small changes in the conductivity. To provide proper timing, the Linac pulse must be delayed relative to the application of the voltage pulse to assure that the voltage turn-on transients have decayed when the Linac pulse arrives at the sample. Referring to Fig. 10, this is accomplished by inserting a delay in the Linac master clock line which provides triggering pulses to the Linac circuits. When

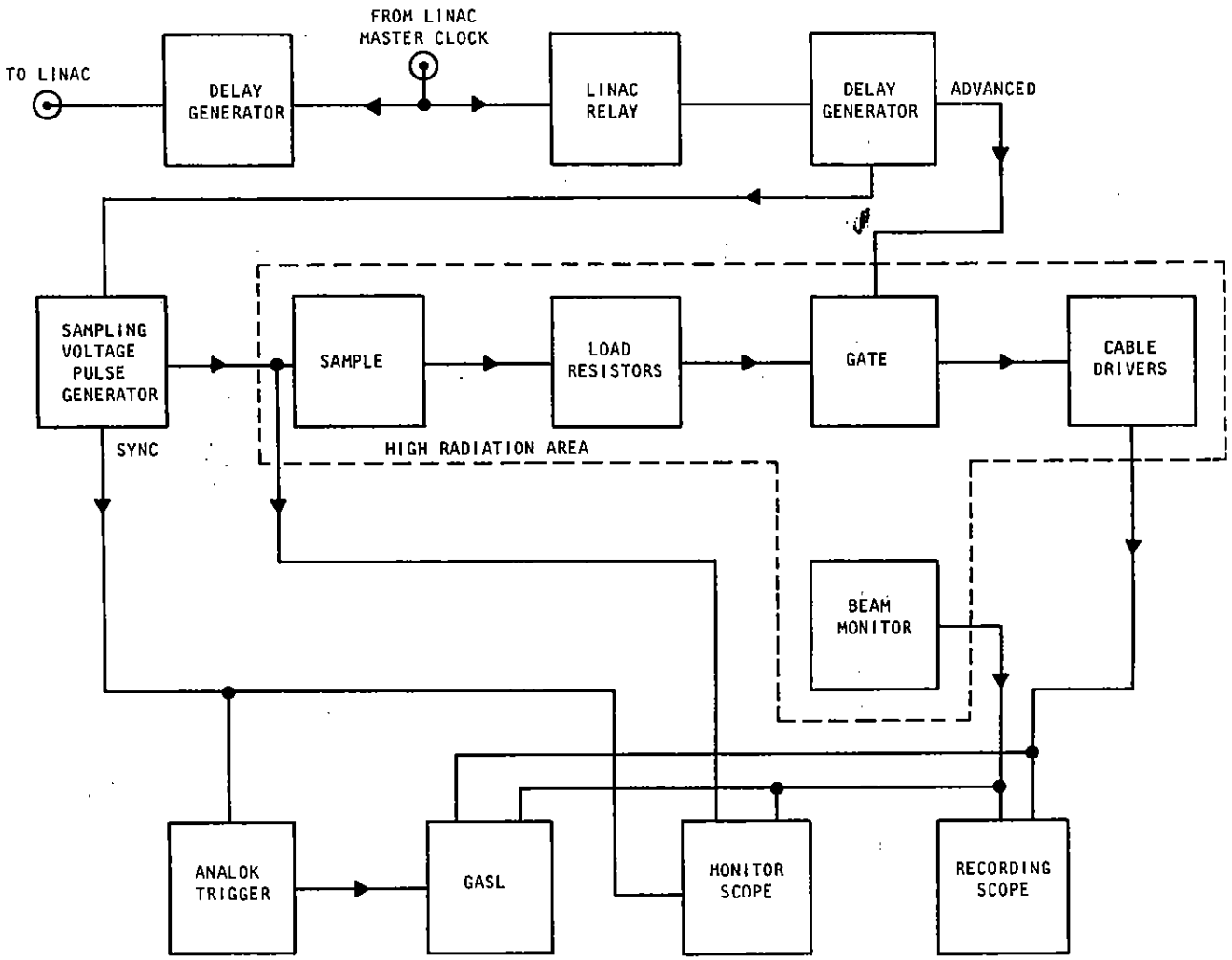

Fig. 10 Schematic of experimental setup at Linac required to perform transient conductivity measurements in concrete

the Linac relay is actuated (by a button on the experimenter's console), a delayed pulse is sent to the injector and an undelayed pulse is used to trigger the experimental apparatus. Adjusting this delay allows the relative timing between Linac pulses, and experimental functions to be adjusted.

To allow the signal amplifiers to operate at high sensitivity when the Linac pulse arrives, a means must be found to prevent the voltage turn-on transient from saturating the inputs. This is accomplished by the use of a gate. Figure 10 shows the location of the gate in the system and Fig. 4 shows the gate schematically. It is comprised of a low-leakage mica capacitor between the load resistor output and the amplifier input. The amplifier side of the capacitor is maintained at ground potential by a normally-closed mercury-wetted relay which is driven by an additional variable-delay pulse generator. After the initial charging transient has arrived and the capacitor is charged to the steady-state voltage across the load resistor, the gate is driven open and any subsequent pulses then are received by the amplifier.

The sequence of events is: (1) application of the voltage pulse, (2) opening of the gate, (3) triggering of the recording equipment, (4) firing of the Linac. This sequence is shown in Fig. 11 relative to the Linac master trigger generator or clock (2). When the command to fire is given (b), a relay is closed which enables the next clock pulse to fire the Linac (c). The delay generator introduced between the clock and the Linac circuits provides a variable delay between the clock pulse and the radiation pulse (d). The clock pulse is also sent through the experimenter's relay and triggers the gate drive pulse generator (e). This pulser is operated in the advance mode because of the relatively long time taken by the mercury-wetted relay to open (f). The applied-voltage pulser is also triggered on the clock pulse and, set on minimum delay, is controlled by the experimenter to provide the desired pulse width and amplitude desired (g). The scope is triggered a few tenths of a microsecond before the Linac injector, and the resulting scope trace appears as in (h).

The recording system is comprised of a primary photographic recording oscilloscope to record the transient conductivity signal and the radiation monitor signal, a monitor scope to display the applied voltage and the radiation monitor signal for timing purposes, and a General Applied Science

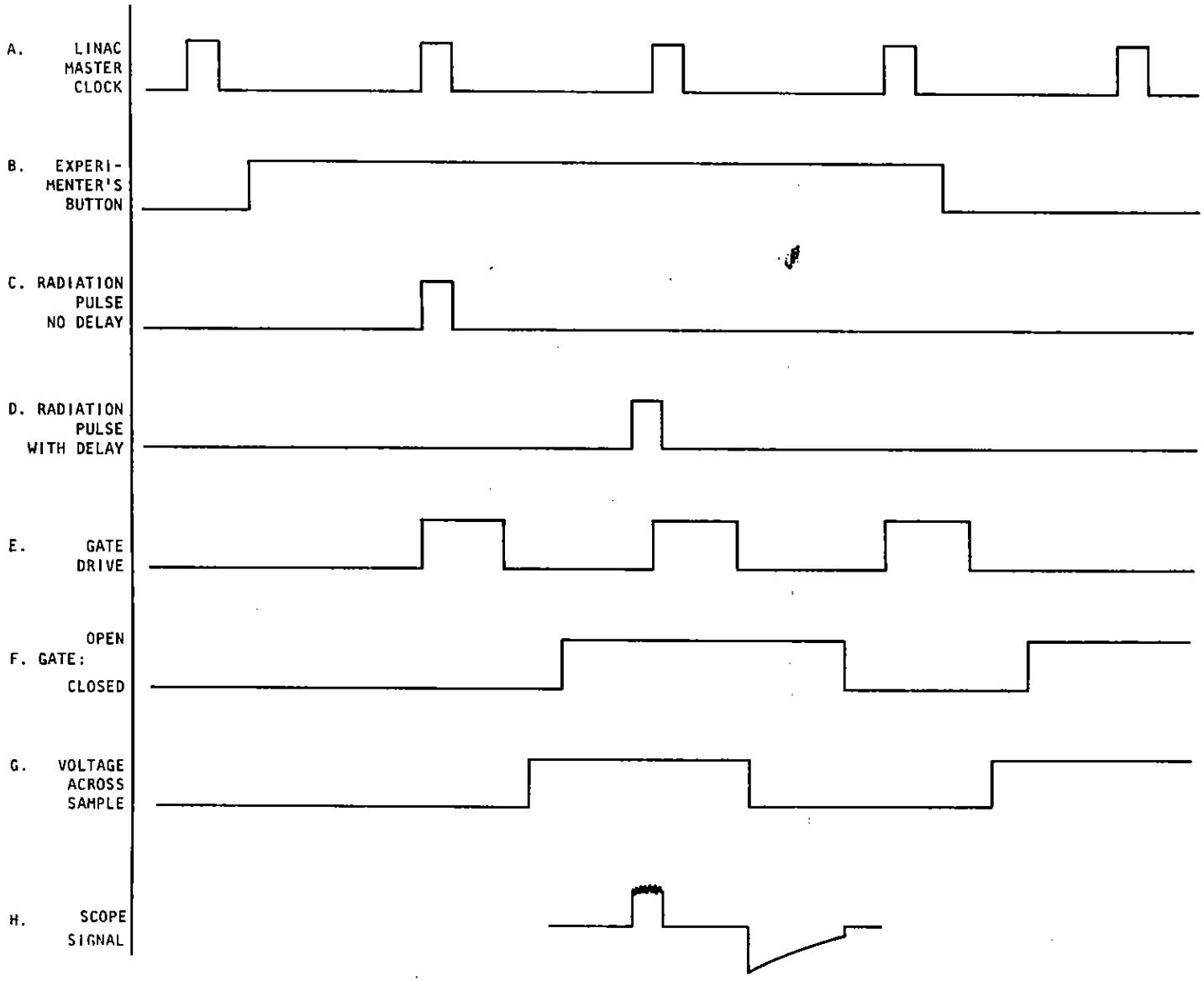

Fig. 11 Schematic of timing pulses occurring in one Linac firing cycle. The vertical and horizontal axes are in arbitrary units.

Laboratory (GASL) data recording system. The GASL system digitizes data in 30 time channels and records it on tape suitable for input by a UNIVAC 1108 computer.

A typical Linac photograph representing one data point is shown as a tracing in Fig. 12, where in (a) the upper trace is the radiation-induced change in the current flowing through the sample with a positive 20-volt pulse applied, and the lower trace is the integrated beam monitor signal which is proportional to the radiation dose delivered; (b) shows the signal obtained with a negative 20-volt pulse applied. The fact that both signals are of the same polarity is because the observed voltage is the sum of the conductivity signal and the secondary electron emission signal. Since the latter is independent of applied bias, the conductivity signal is computed by subtracting the (+) and (-) bias signals, normalized to their respective beam monitor amplitudes.

The conductivity is then computed using the dimensions of the samples and the voltage across the sample.

4.3.2 Temperature Dependence of the Transient Conductivity

Figure 13 shows the transient conductivity for several samples as a function of temperature. The data points are normalized to 10^{10} rad/sec, using a 4-μsec pulse width. The vacuum-dry samples and the dry samples show monotonically increasing conductivity with increasing temperature. However, the activation energy for the radiation-induced conductivity (RIC) is much smaller than for the ambient conductivity. This is to be expected, since the ambient conductivity data reflect the temperature dependence of the ion concentration, while the RIC data reflect the temperature dependence of the lifetime of the enhanced concentrations of carriers.

The scatter in the data reflects the differences in the makeup of the samples.

The RIC in the wet samples is seen to increase with temperature at low temperatures and then to decrease at higher temperatures.

The scatter in the data is considered small in view of the variations in water content (porosity) in the samples which make up an experimental sample, and, with the exception of a very dry sample (WE-2, curve A), the low-temperature transient conductivities of all the samples, wet and dry,

(a)

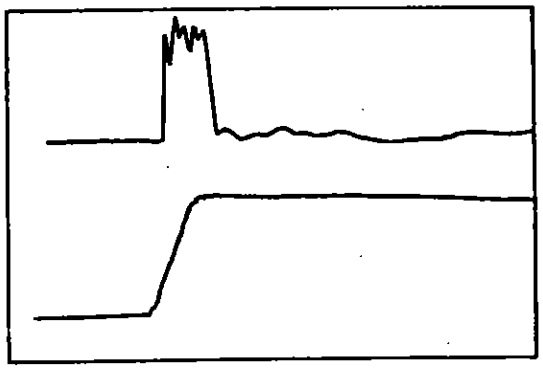

UPPER: 10^{-3} amp/cm
LOWER: 5 volts/cm
SWEEP: 5 μsec/cm
APPLIED VOLTAGE: +20

(b)

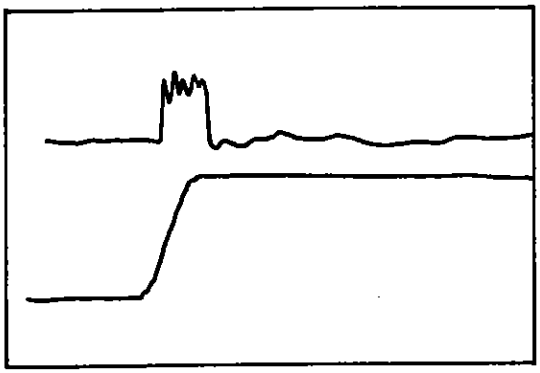

UPPER: 10^{-3} amp/cm
LOWER: 5 volts/cm
SWEEP: 5 μsec/cm
APPLIED VOLTAGE: - 20

Fig. 12 Tracing of typical oscilloscope photographs showing (a) the change in the current flowing through the sample during a Linac pulse; the integrated monitor signal giving the delivered radiation dose. The applied voltage was positive 20 volts. (b) The same as (a) but an applied voltage of negative 20 volts.

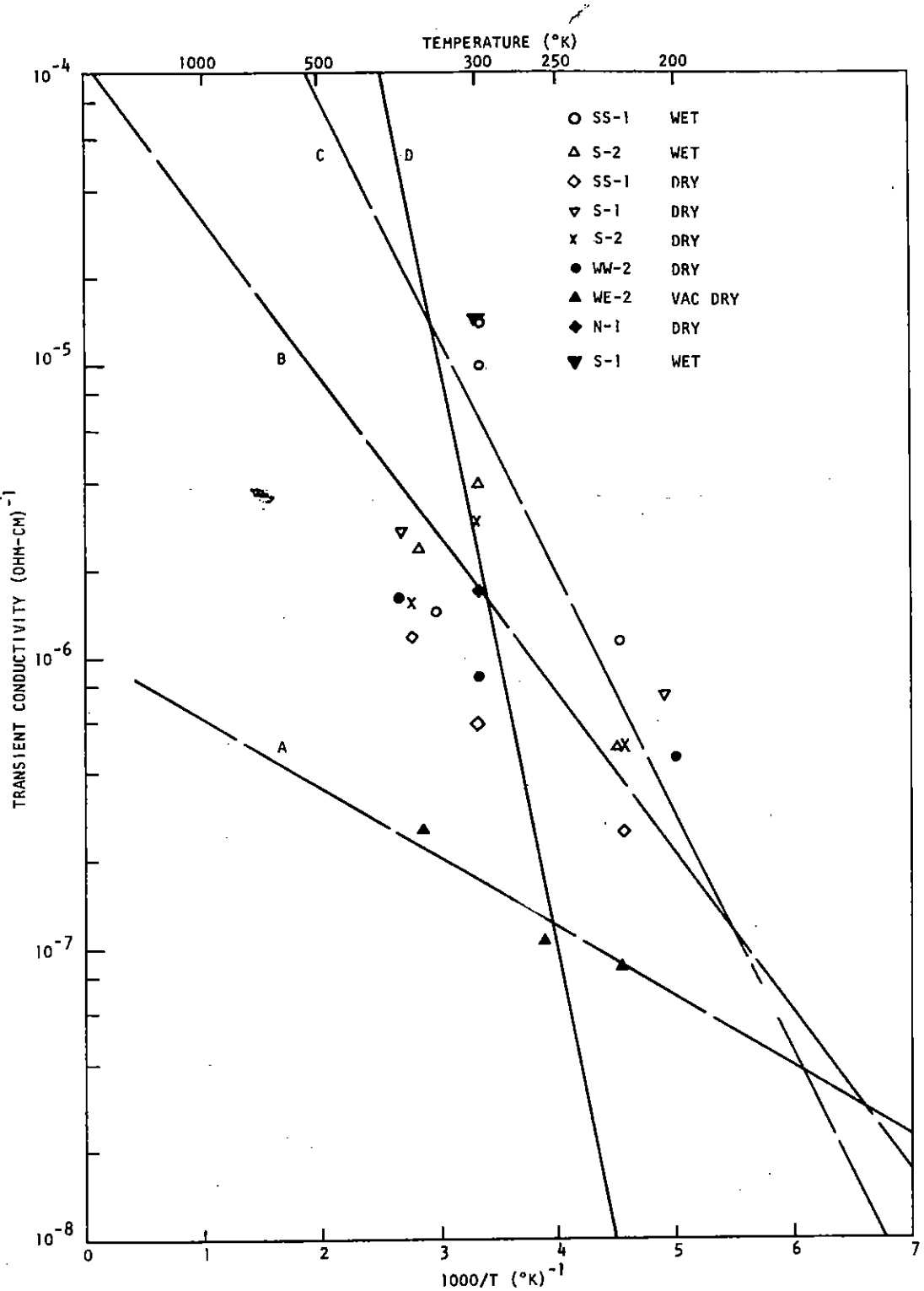

Fig. 13 Transient conductivity as a function of reciprocal temperature for all samples. The data points represent the least-squares value of the transient conductivity at 10^{10} rads/sec. Curve A shows the behavior of a very dry sample (WE-2-1, WE-2-2); Curve B shows the average of the +20°C and -50°C data for all the dry samples; Curve C is the average of the +20°C and -50°C data for the wet samples; Curve D is the ambient conductivity of a dry sample (WW-2-1, WW-2-2).

fall within a factor of 5 of each other. Because the samples were initially chosen for their low inhomogeneity, their porosity, which is the determining factor in their water content, was expected to be reasonably similar. In fact, however, the water contents of even adjacent samples were found to differ by a considerable amount. The conductivity is, therefore, representative of two parallel samples of different water content and the data must be interpreted accordingly.

Figure 14 shows the transient conductivity versus the reciprocal temperature for two samples of the same water content. Curve A is the conductivity of the dry composite sample (WW-2-1, WW-2-2) with a moisture content of 1.2%, and was measured at a constant dose rate of 6.2×10^9 rad/sec; curve B is the conductivity of the dry composite sample (S-1-2, S-1-3) with moisture contents of 0.7% and 1.2%, respectively, and was measured at a constant dose rate of 5.9×10^9 rad/sec. A least-squares fit of all the data points to the equation $\sigma_p = \sigma_0 \exp(-E/kT)$ obtains

$$\text{Curve A} \quad \sigma_p = 11.1 \times 10^{-6} \exp(-0.76/kT),$$
$$\text{Curve B} \quad \sigma_p = 5.69 \times 10^{-6} \exp(-0.64/kT).$$

4.3.3 Dose-Rate Dependence

Measurements of the transient conductivity as a function of dose rate were performed on five pairs of samples with moisture contents in the 0.9 to 1.5% range which corresponds to the moisture content in equilibrium with a relative humidity of 40% to 50% at ~20°C, and on three pairs of samples with water contents in the 4 to 7% range.

4.3.3.1 Ambient and Dry Samples. Each of the curves shown in Figs. 15 through 20 corresponds to the transient conductivity versus dose rate at a particular temperature within the specified range -50°C to +100°C, and is a least-squares fit of the data to the equation

$$\sigma_p = \sigma_0 (\dot{\gamma})^{\Delta} ,$$

where σ_0 and Δ are fitting parameters.

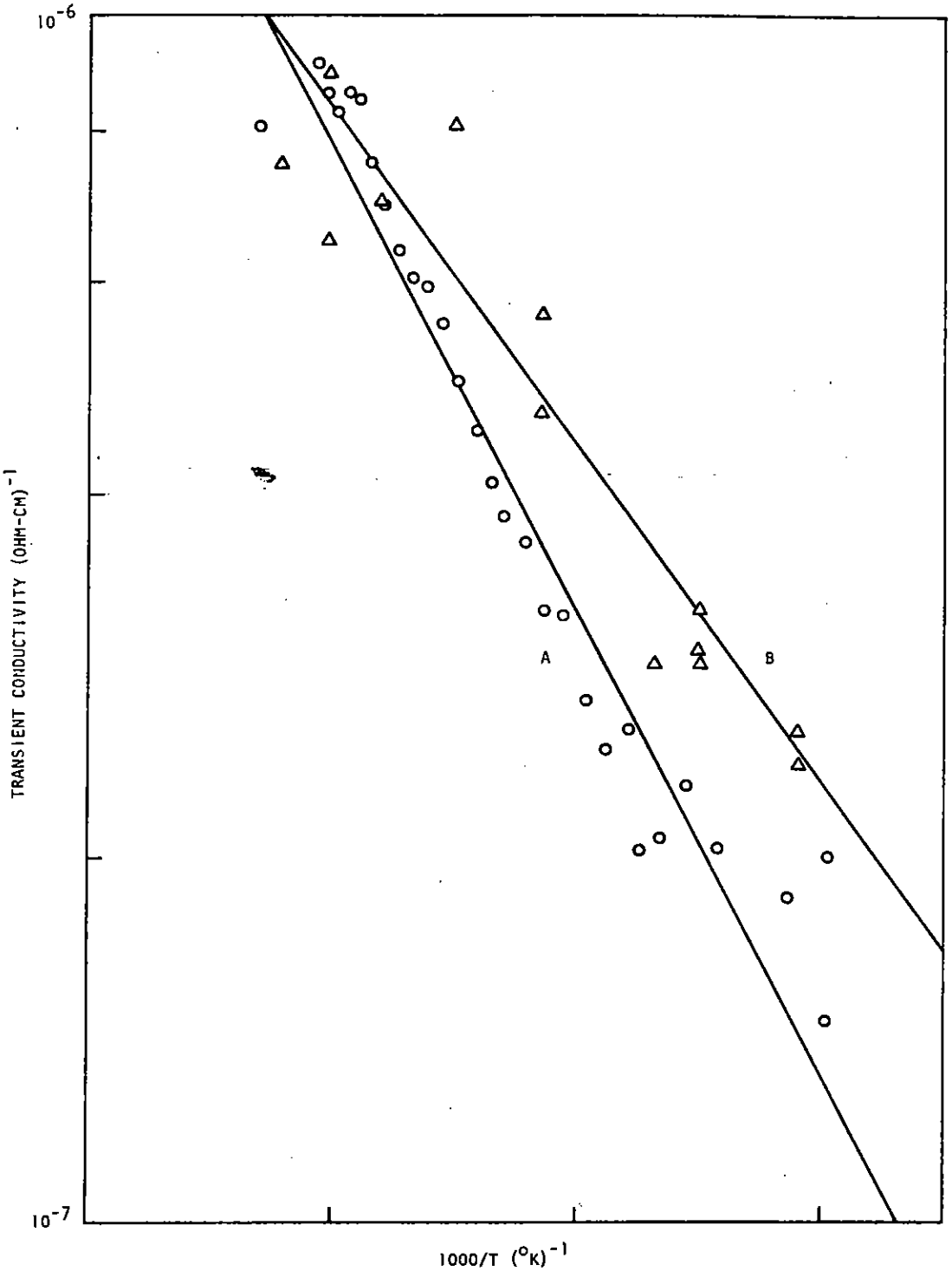

Fig. 14 Transient conductivity at constant dose as a function of reciprocal temperature. Curve A shows a composite sample (WW-2-1, WW-2-2) with 1.2% water by weight at a constant dose-rate of 6.2×10^9 rads/sec. Curve B shows a composite sample (S-1-2,S-1-3), 1% water by weight, at a constant dose-rate of 5.9×10^9 rads/sec. The conductivities are (Curve A) $\sigma_p = 11.1 \times 10^{-6} \exp(-0.76/kT)$ and (Curve B) $\sigma_p = 5.7 \times 10^{-6} \exp(-0.64/kT)$.

Figure 15 shows the transient conductivity as a function of dose rate of a dry composite sample (SS-1-2, SS-1-3), containing, respectively, 1.2% and 1.6% water by weight. The data points on curve A at 9×10^9 rad/sec were taken at two temperatures. The open circles belong to curve A and correspond to a temperature of 87°C; the open triangles on curve A belong to curve B and were taken at a temperature of ~35°C. Curve B, which is the remaining data, was taken at a sample temperature between ~0°C and -5°C. This was a result of a temperature control malfunction.

The functions describing the conductivity are

$$\text{Curve A} \quad 87^\circ\text{C} \quad \sigma_p = 5.2 \times 10^{-13} (\dot{\gamma})^{0.64} \quad ,$$
$$\text{Curve B} \quad 20^\circ\text{C} \quad \sigma_p = 5.6 \times 10^{-15} (\dot{\gamma})^{0.80} \quad ,$$
$$\text{Curve C} \quad -49^\circ\text{C} \quad \sigma_p = 6.8 \times 10^{-14} (\dot{\gamma})^{0.66} \quad .$$

Figure 16 shows a well-behaved dry sample (WW-2-1, WW-2-2) containing ~1.2% water by weight. The transient conductivity versus dose-rate curves indicate a very similar conductivity behavior to that in Fig. 15.

The equations describing the transient conductivity are

$$98^\circ\text{C} \quad \sigma_p = 1.1 \times 10^{-12} (\dot{\gamma})^{0.62} \quad ,$$
$$20^\circ\text{C} \quad \sigma_p = 2.2 \times 10^{-15} (\dot{\gamma})^{0.86} \quad ,$$
$$-70^\circ\text{C} \quad \sigma_p = 1.6 \times 10^{-14} (\dot{\gamma})^{0.74} \quad .$$

Figure 17 shows the transient conductivity versus dose rate for a dry sample (S-2-1, S-2-3) containing 1.5% and 2.4% water by weight. In these samples, the transient conductivity is seen to have a shallower dose-rate dependence at 87°C than at the lower temperatures, and at high dose rates, the high temperature curve is actually below the 20°C curve.

The equations describing the transient conductivity are

$$\text{Curve A} \quad 87^\circ\text{C} \quad \sigma_p = 1.9 \times 10^{-13} (\dot{\gamma})^{0.69} \quad ,$$
$$\text{Curve B} \quad 20^\circ\text{C} \quad \sigma_p = 2.4 \times 10^{-15} (\dot{\gamma})^{0.91} \quad ,$$
$$\text{Curve C} \quad -53^\circ\text{C} \quad \sigma_p = 2.8 \times 10^{-14} (\dot{\gamma})^{0.72} \quad .$$

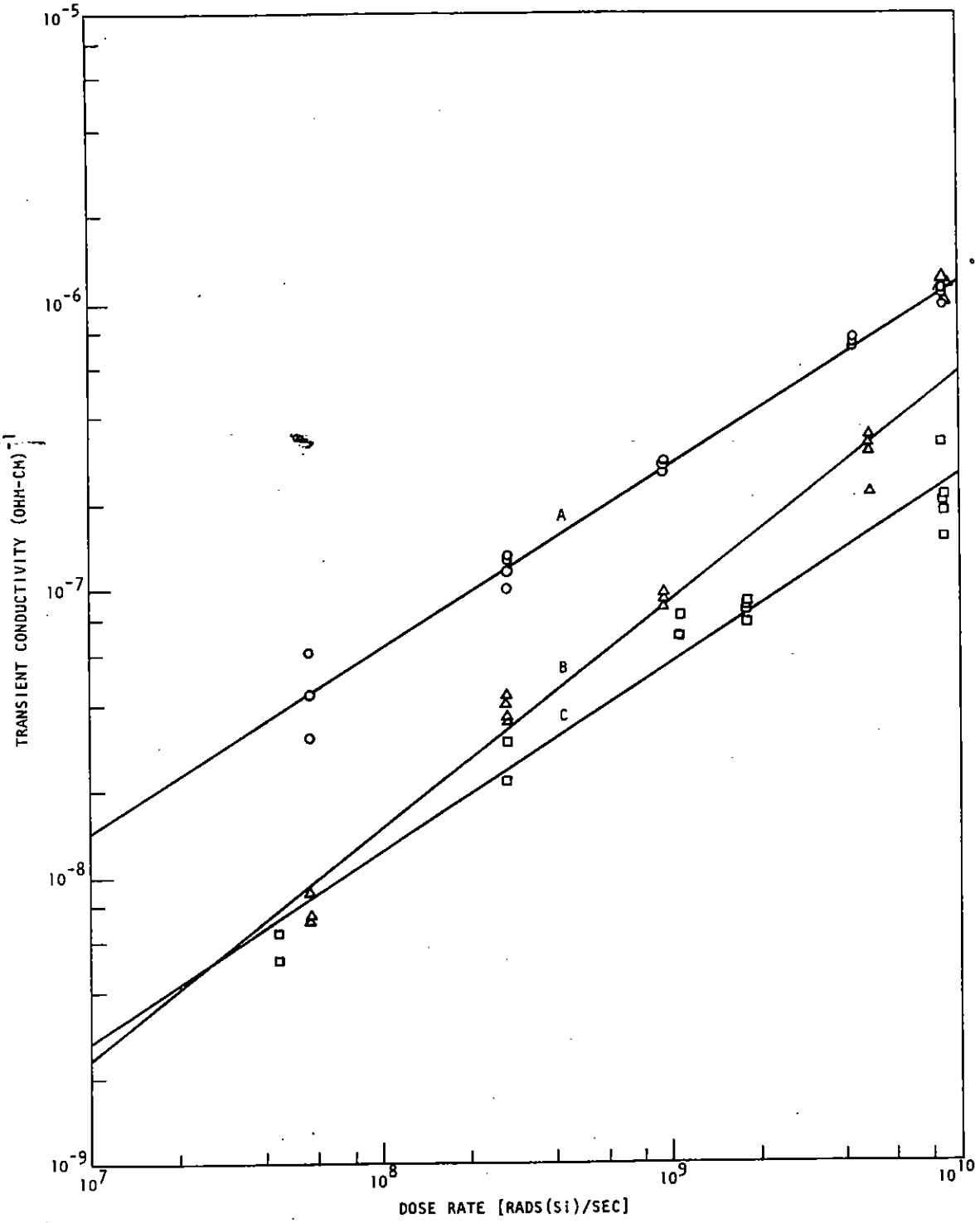

Fig. 15 Transient conductivity as a function of dose-rate for dry sample (SS-1-2, SS-1-3) containing 1.2% and 1.6% water by weight. (Curve A) 87 C, $\sigma_p = 5.2 \times 10^{-13} (\dot{\gamma})^{0.64}$; (Curve B) ~0° C, $\sigma_p = 5.6 \times 10^{-15} (\dot{\gamma})^{0.80}$; (Curve C) -49° C, $\sigma_p = 6.8 \times 10^{-14} (\dot{\gamma})^{0.66}$.

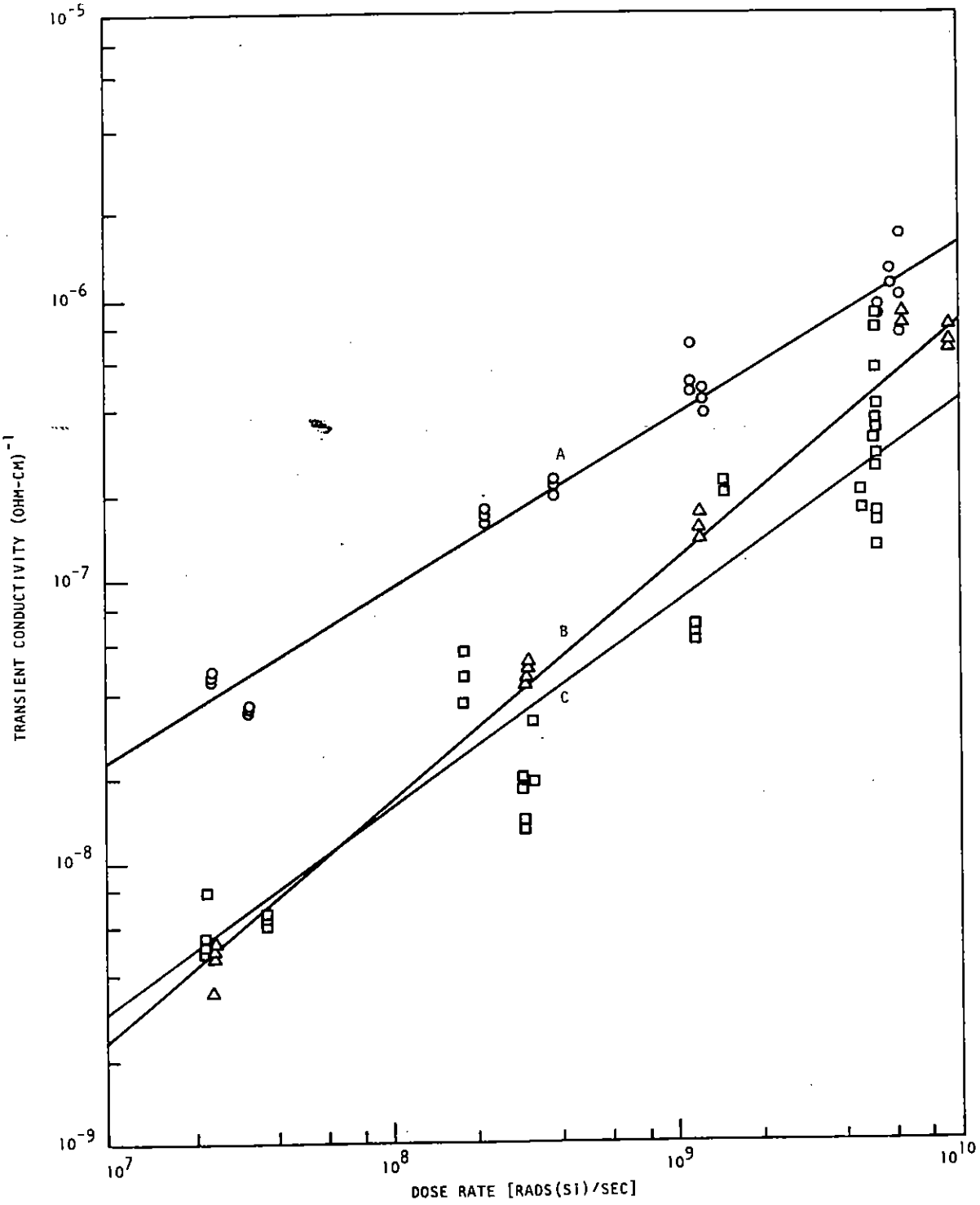

Fig. 16 Transient conductivity as a function of dose rate for dry sample (WW-2-1, WW-2-2) containing 1.2% water by weight. (Curve A) 98°C, $\sigma_p = 1.1 \times 10^{-12}(\dot{\gamma})^{0.62}$; (Curve B) 20°C, $\sigma_p = 2.2 \times 10^{-15}(\dot{\gamma})^{0.86}$; (Curve C) -70°C, $\sigma_p = 1.6 \times 10^{-14}(\dot{\gamma})^{0.74}$.

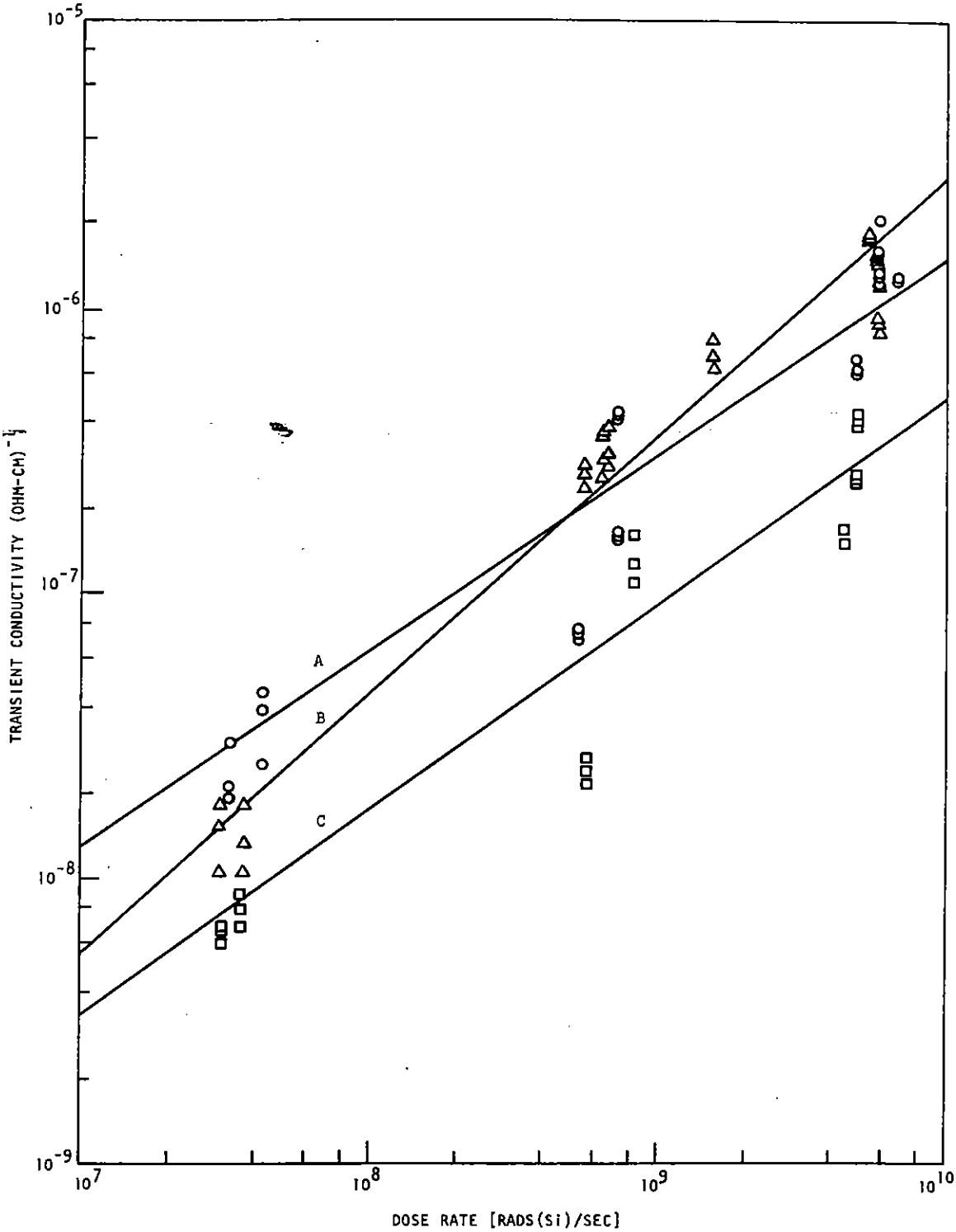

Fig. 17 Transient conductivity as a function of dose rate for dry sample (S-2-1,S-2-3) containing 1.5% and 2.4% water by weight. (Curve A) 87°C, $\sigma_p = 1.9 \times 10^{-13}(\dot{\gamma})^{0.69}$; (Curve B) 20°C, $2.4 \times 10^{-15}(\dot{\gamma})^{0.91}$; (Curve C) -53°C, $\sigma_p = 2.8 \times 10^{-14}(\dot{\gamma})^{0.72}$.

Figure 18 represents the transient conductivity versus dose rate for a dry composite sample (S-1-2, S-1-3) containing 0.7% and 1.2% water by weight. Note that in these composite samples the high-temperature conductivity is definitely depressed below that at room temperature. The equations of the transient conductivity are

$$\text{Curve A} \quad 93^\circ\text{C} \quad \sigma_p = 5.7 \times 10^{-14} (\dot{\gamma})^{0.76} \ ,$$

$$\text{Curve B} \quad 20^\circ\text{C} \quad \sigma_p = 2.8 \times 10^{-13} (\dot{\gamma})^{0.70} \ ,$$

$$\text{Curve C} \quad -68^\circ\text{C} \quad \sigma_p = 1.1 \times 10^{-14} (\dot{\gamma})^{0.78} \ .$$

Figure 19 shows the transient conductivity versus dose rate for several constant doses in a dry sample (S-1-2, S-1-3). The temperature of the sample was 20° C. The data points, which correspond to the values of dose indicated in the figure, fit reasonably well to the straight line which is the equation of the transient conductivity at 20° C shown in Fig. 18. It can be seen that, even for constant dose points, the conductivity is not linear in the dose rate.

Figure 20 shows the transient conductivity versus dose rate for a sample (WE-2-1, WE-2-2) in a very dry condition. The estimated moisture content is <0.01% water by weight. The low value of σ_0 reflects the small contribution to the conductivity of the ions in solution.

The equations of the transient conductivity are

$$\text{Curve A} \quad 70^\circ\text{C} \quad \sigma_p = 2.5 \times 10^{-18} (\dot{\gamma})^{1.2} \ ,$$

$$\text{Curve B} \quad 16^\circ\text{C} \quad \sigma_p = 3.4 \times 10^{-19} (\dot{\gamma})^{1.2} \ ,$$

$$\text{Curve C} \quad -53^\circ\text{C} \quad \sigma_p = 2.1 \times 10^{-19} (\dot{\gamma})^{1.2} \ .$$

The superlinear dependence of the RIC on dose rate is not unknown in photoconductors,[6] but the detailed explanation is outside the scope of this report, since detailed knowledge of the energy levels is required to properly describe the microscopic behavior which leads to this dependence. Contrasted with the samples with significant moisture content, the 16° C and -53° C data are quite similar. Even the high-temperature run shows the same slope as the other temperatures, indicating that the water present in the other samples dominates the temperature dependence.

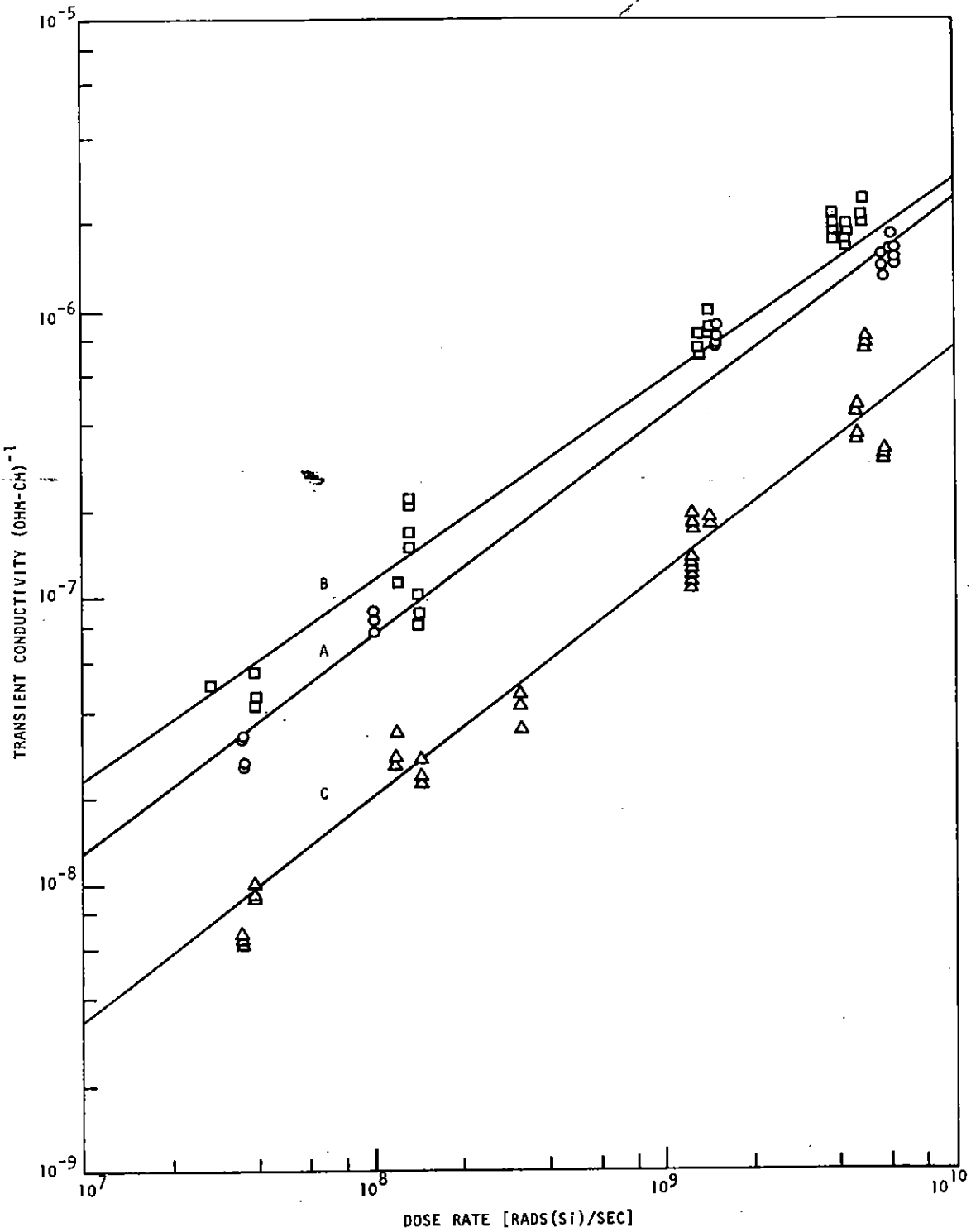

Fig. 18 Transient conductivity as a function of dose rate for dry sample (S-1-2, S-1-3) containing 0.7% and 1.2% water by weight. (Curve A) 93°C, $\sigma_p = 5.7 \times 10^{-14} (\dot{\gamma})^{0.76}$; (Curve B) 20°C, $\sigma_p = 2.8 \times 10^{-13} (\dot{\gamma})^{0.70}$; (Curve C) -68°C, $\sigma_p = 1.1 \times 10^{-14} (\dot{\gamma})^{0.78}$.

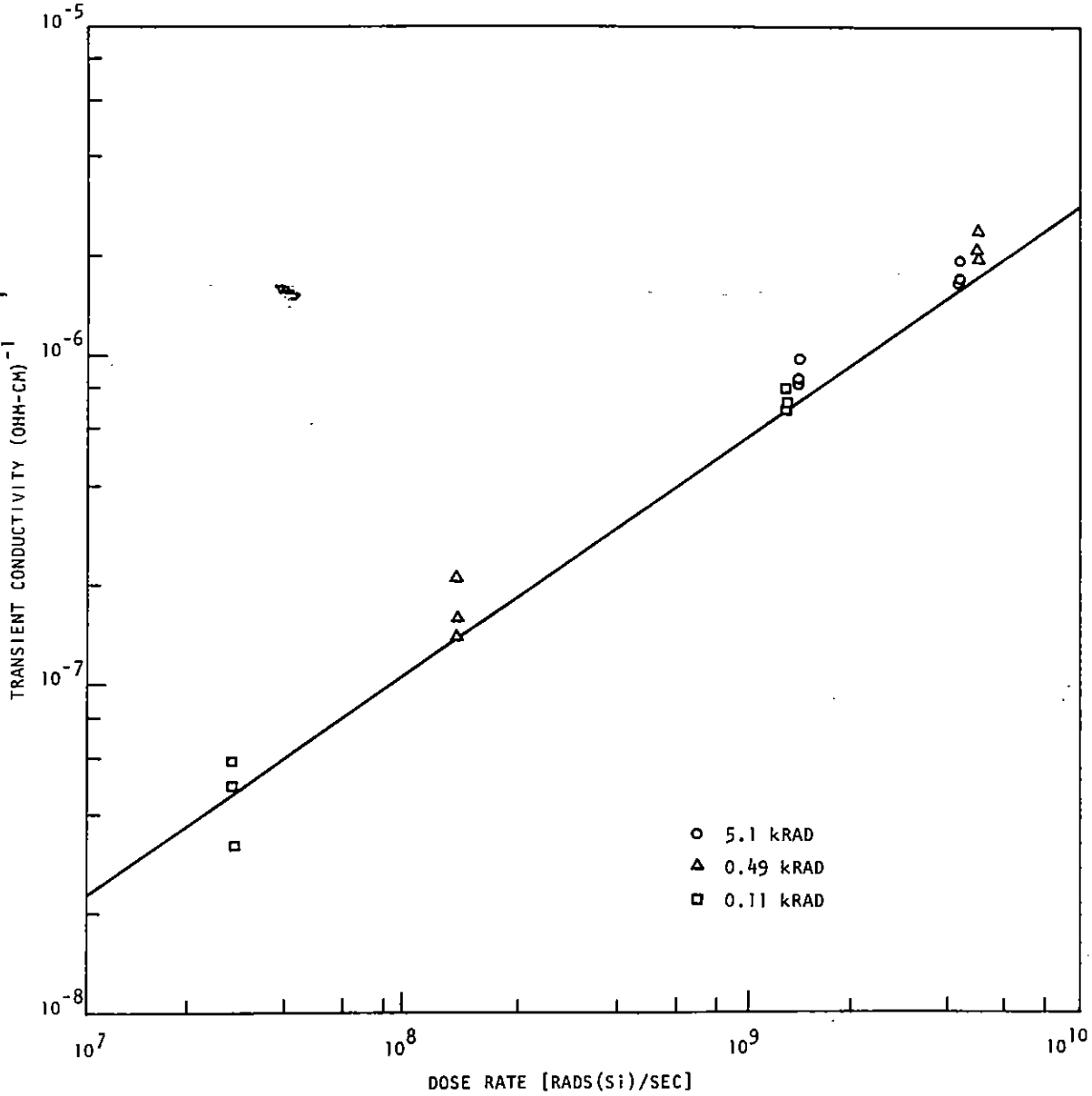

Fig. 19 Transient conductivity as a function of dose rate at constant dose for dry sample (S-1-2, S-1-3) at 20°C. The straight line is the least-squares fit to the data for all doses and dose rates.

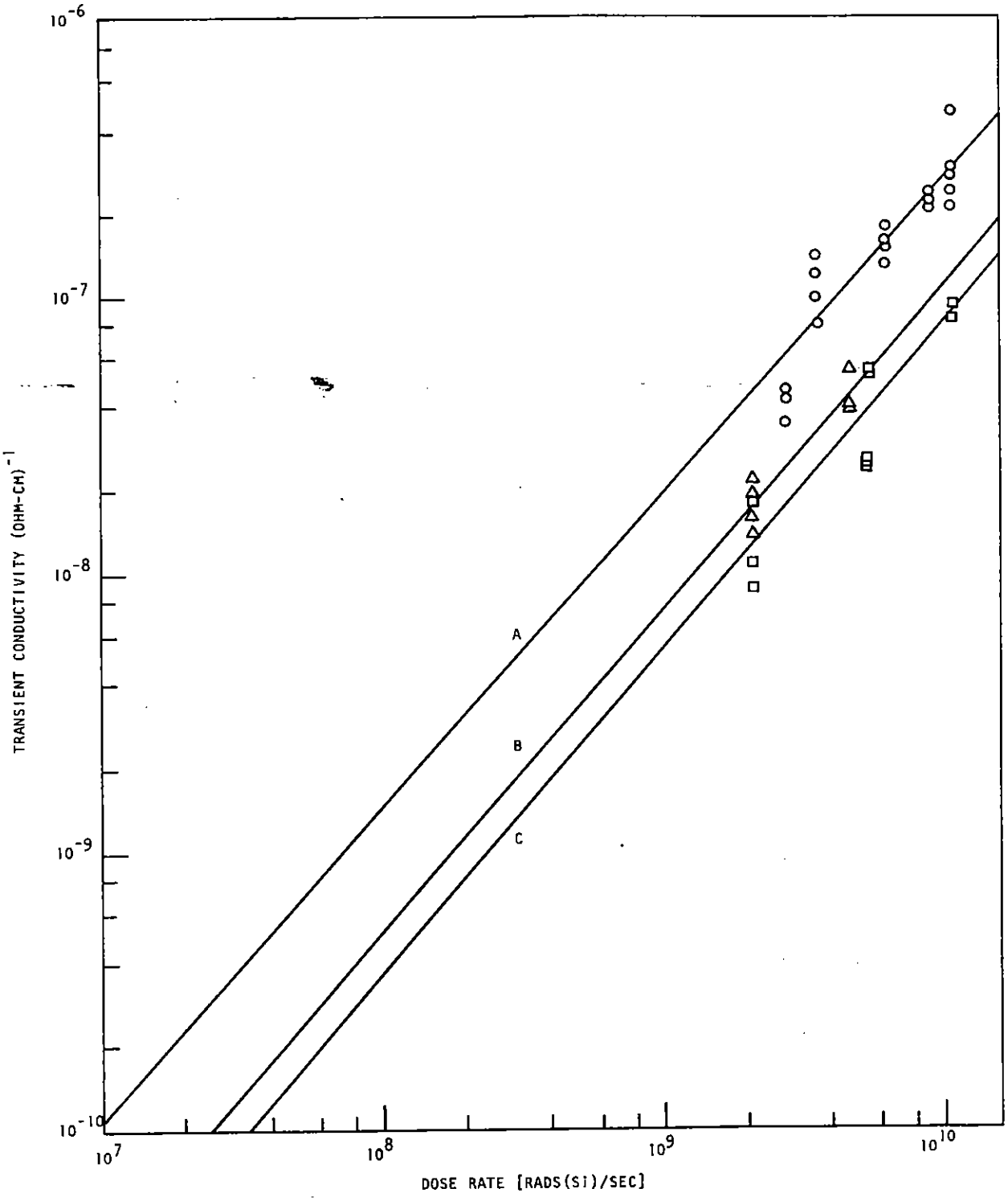

Fig. 20 Transient conductivity as a function of dose rate for very dry sample (WE-2-1, WE-2-2). (Curve A) 70°C, $\sigma_p = 2.5 \times 10^{-18} (\dot{\gamma})^{1.2}$; (Curve B) 16°C, $\sigma_p = 3.4 \times 10^{-19} (\dot{\gamma})^{1.2}$; (Curve C) -53°C, $\sigma_p = 2.1 \times 10^{-19} (\dot{\gamma})^{1.2}$.

4.3.3.2 Wet Concrete. In Fig. 21, the transient conductivity as a function of dose rate is shown for a composite sample (S-2-1, S-2-3) containing, respectively, 4.6% and 6.1% water by weight. The transient conductivity relationships are

$$\text{Curve A} \quad 79^\circ\text{C} \quad \sigma_p = 1.6 \times 10^{-14} (\dot{\gamma})^{0.82} \ ,$$

$$\text{Curve B} \quad 20^\circ\text{C} \quad \sigma_p = 1.2 \times 10^{-12} (\dot{\gamma})^{0.65} \ ,$$

$$\text{Curve C} \quad -53^\circ\text{C} \quad \sigma_p = 1.6 \times 10^{-14} (\dot{\gamma})^{0.75} \ .$$

The data points are included to show the small amount of scatter and the good fit to the computed straight line.

A second wet sample, composed of (SS-1-2, SS-1-3) with, respectively, 5.7% and 5.1% moisture, produced quite different results. Figure 22 shows the transient conductivity versus dose rate at a sample temperature of 20°C. The data points, many of which fall on each other, indicate a definite rollover at high dose rates. A least-squares fit to the entire data produces the relationship shown in curve A, or

$$\sigma_p = 3.0 \times 10^{-18} (\dot{\gamma})^{1.18} \ .$$

If the high-dose-rate data are considered too low and are not included in the least-squares analysis, the relationship shown in Curve B becomes

$$\sigma_p = 2.5 \times 10^{-21} (\dot{\gamma})^{1.56} \ .$$

The roll-off at high dose rates was also observed at low temperatures. Figure 23 shows the transient conductivity versus dose rate for the same sample at ~-50°C. The best fit to the data gives the curve A, for which

$$\sigma_p = 1.02 \times 10^{-14} (\dot{\gamma})^{0.81} \ ,$$

while exclusion of the high-dose-rate data gives curve B or

$$\sigma_p = 2.8 \times 10^{-17} (\dot{\gamma})^{1.16} \ .$$

The data points near 10^{-6} $(\text{ohm-cm})^{-1}$ were taken at a dose rate of $\sim 4.4 \times 10^{9}$ $\dot{\gamma}$ and with a radiation pulse width of 0.1 μsec. The charging transient was much larger in these wet samples than that dealt with in

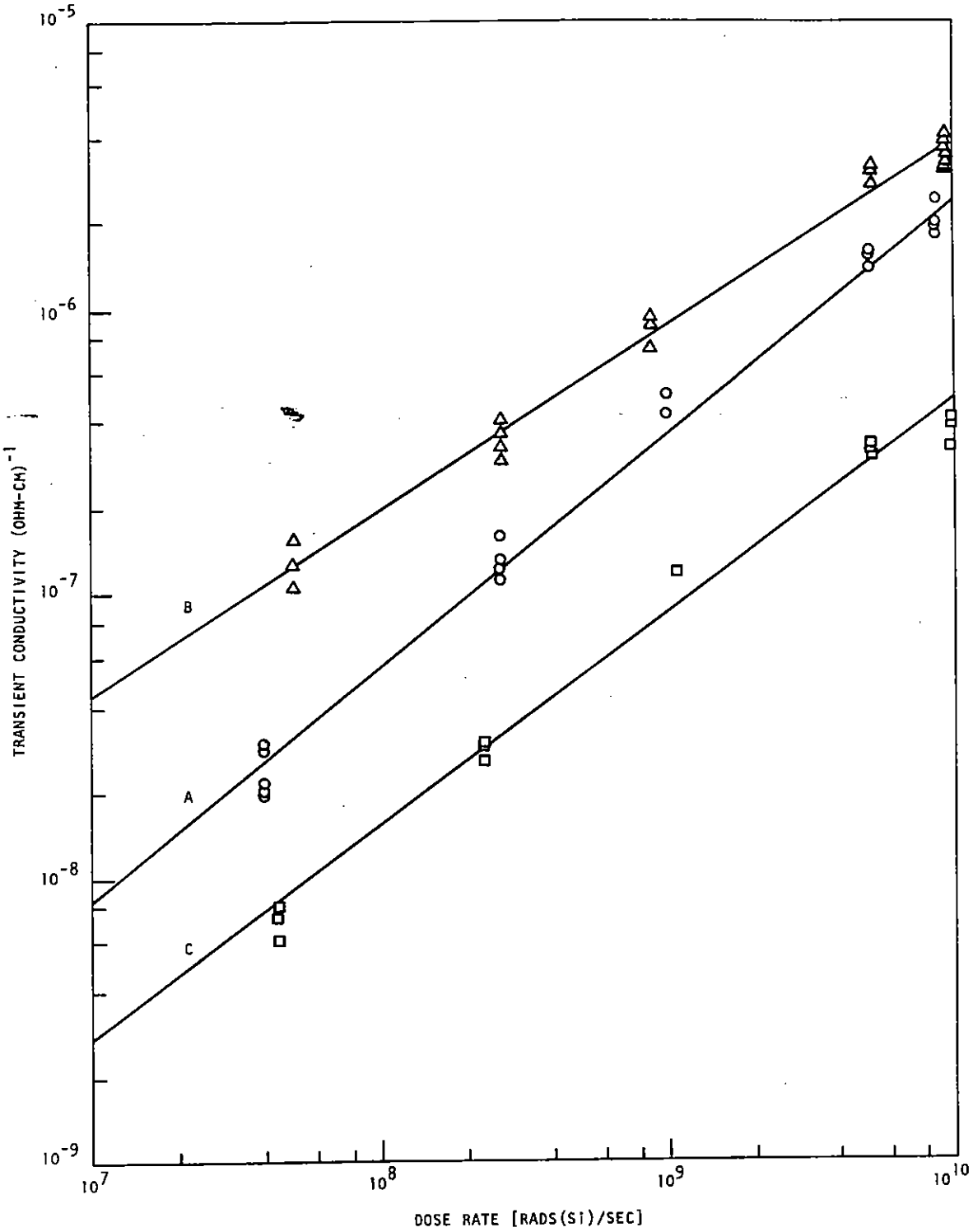

Fig. 21 Transient conductivity as a function of dose rate for wet sample (S-2-1, S-2-3) containing 4.6% and 6.1% water, respectively. (Curve A) 79 C, $\sigma_p = 1.6 \times 10^{-14} (\dot{\gamma})^{0.82}$; (Curve B) 20°C, $\sigma_p = 1.2 \times 10^{-12} (\dot{\gamma})^{0.65}$; (Curve C) -53°C, $\sigma_p = 1.6 \times 10^{-14} (\dot{\gamma})^{0.75}$.

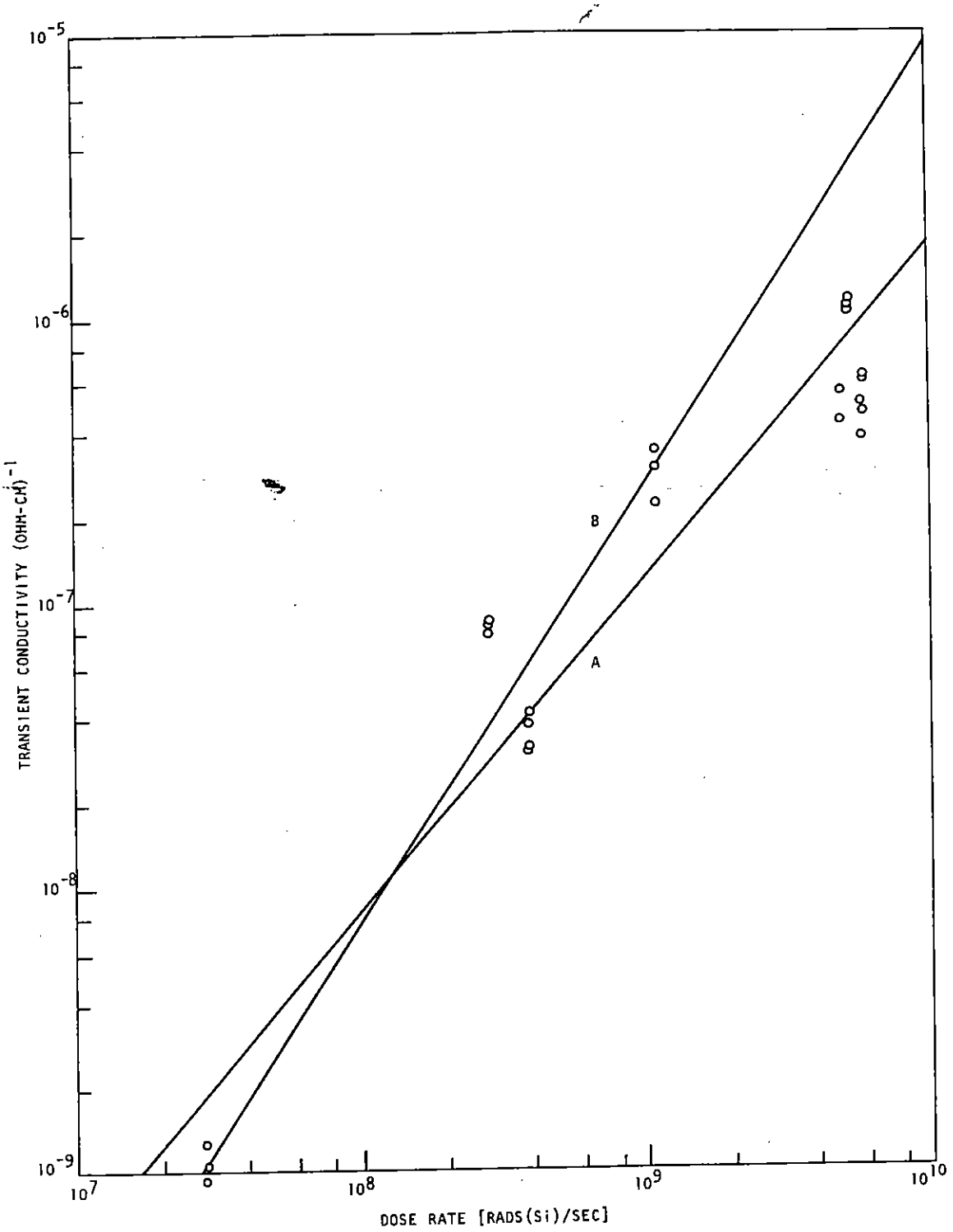

Fig. 22 Transient conductivity as a function of dose rate for wet sample (SS-1-2, SS-1-3) containing 5.7% and 5.1% water by weight, respectively, at 20°C. (Curve A) least-squares fit to all the data, $\sigma_p = 3.0 \times 10^{-18}(\dot{\gamma})^{1.18}$; (Curve B) least-squares fit to the low dose rate data, $\sigma_p = 2.5 \times 10^{-21}(\dot{\gamma})^{1.56}$.

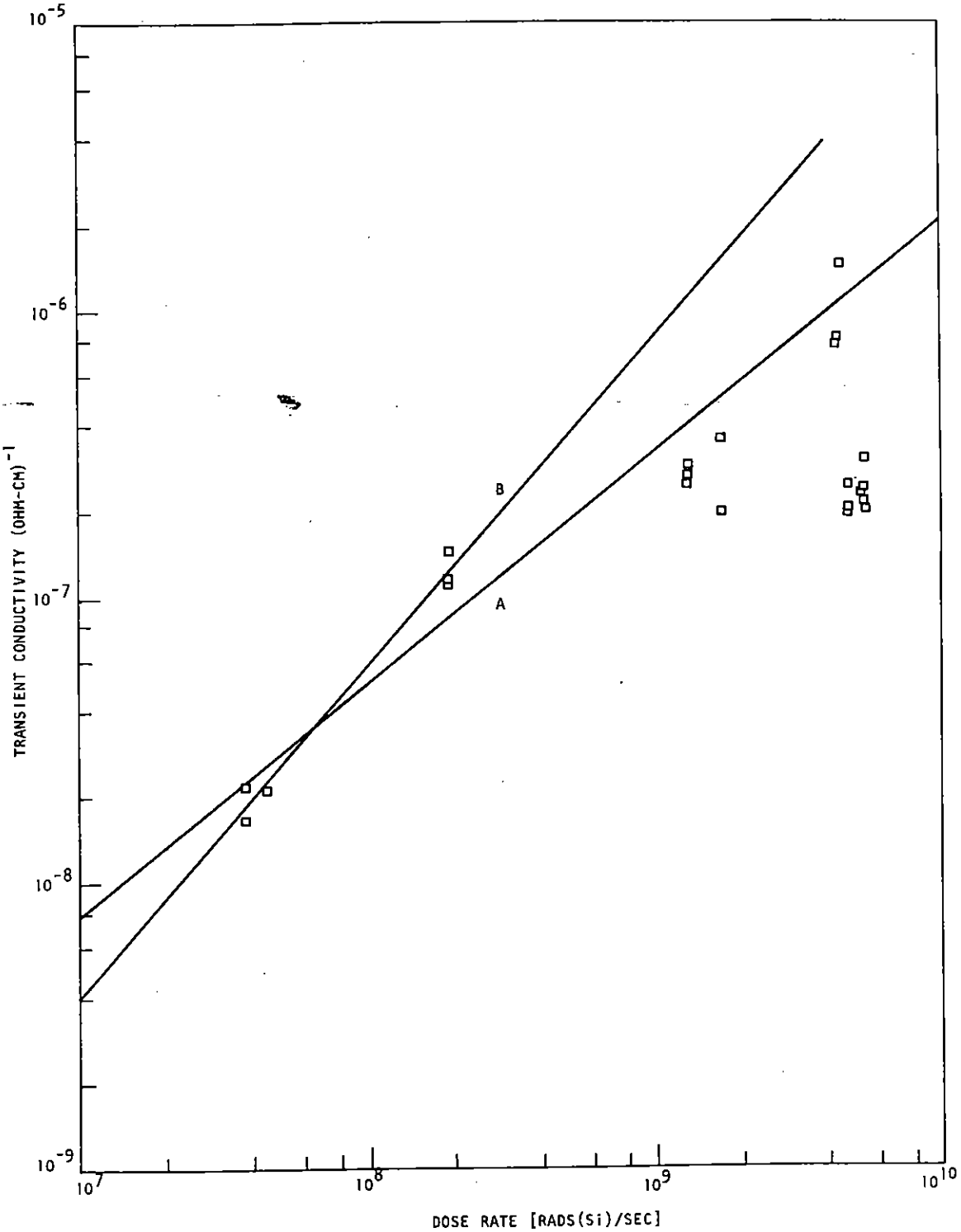

Fig. 23 Transient conductivity as a function of dose rate for wet sample (SS-1-2, SS-1-3) at -50° C. (Curve A) least-squares fit to all the data, $\sigma_p = 1.02 \times 10^{-14}(\dot{\gamma})^{0.81}$; (Curve B) low dose rate data only, $\sigma_p = 2.8 \times 10^{-17}(\dot{\gamma})^{1.16}$.

other samples, and measurements of the transient conductivity could not be performed at temperatures much greater than 62°C.

Figure 24 shows the transient conductivity versus dose rate for a wet sample (SS-1-2, SS-1-3) at 62°C. The best fit through the data gives

$$\sigma_p = 1.0 \times 10^{-17} (\dot{\gamma})^{1.12} \quad .$$

The high-temperature data produce a conductivity versus dose-rate curve which, by comparison, can be seen to be of lower value than those obtained at lower temperatures. Although no definite correlation of the data points to the applied voltage was found, the high-temperature results strongly suggest a space-charge effect.

The question to be addressed is then: Is this behavior representative of wet concrete as a peculiarity of this experiment? The previous sample suggests that the problems are experimental, and to test this, a four-probe measurement was designed.

4.4.4 Four-Probe Measurements

The uncertainty in the results of one of the wet samples and the possibility of degradation effects in the electrodes resulted in the implementation of a method to make four-probe measurements of the transient conductivity in concrete. The four-probe technique is used to measure the potential drop across a length of a sample at a position where the current density is uniform and not electrode-dependent.

The necessary sample holder modifications were made to accomodate a third piece of concrete, the same size as those used in the previous work, and to provide the additional electrical leads required. Because the transient change in the potential had to be probed on a microsecond time scale with a minimum of current being drawn, a very high-input impedance, radiation-hard, differential cathode-follower was built and tested as a buffer stage between the sample and the cable-driving amplifiers.

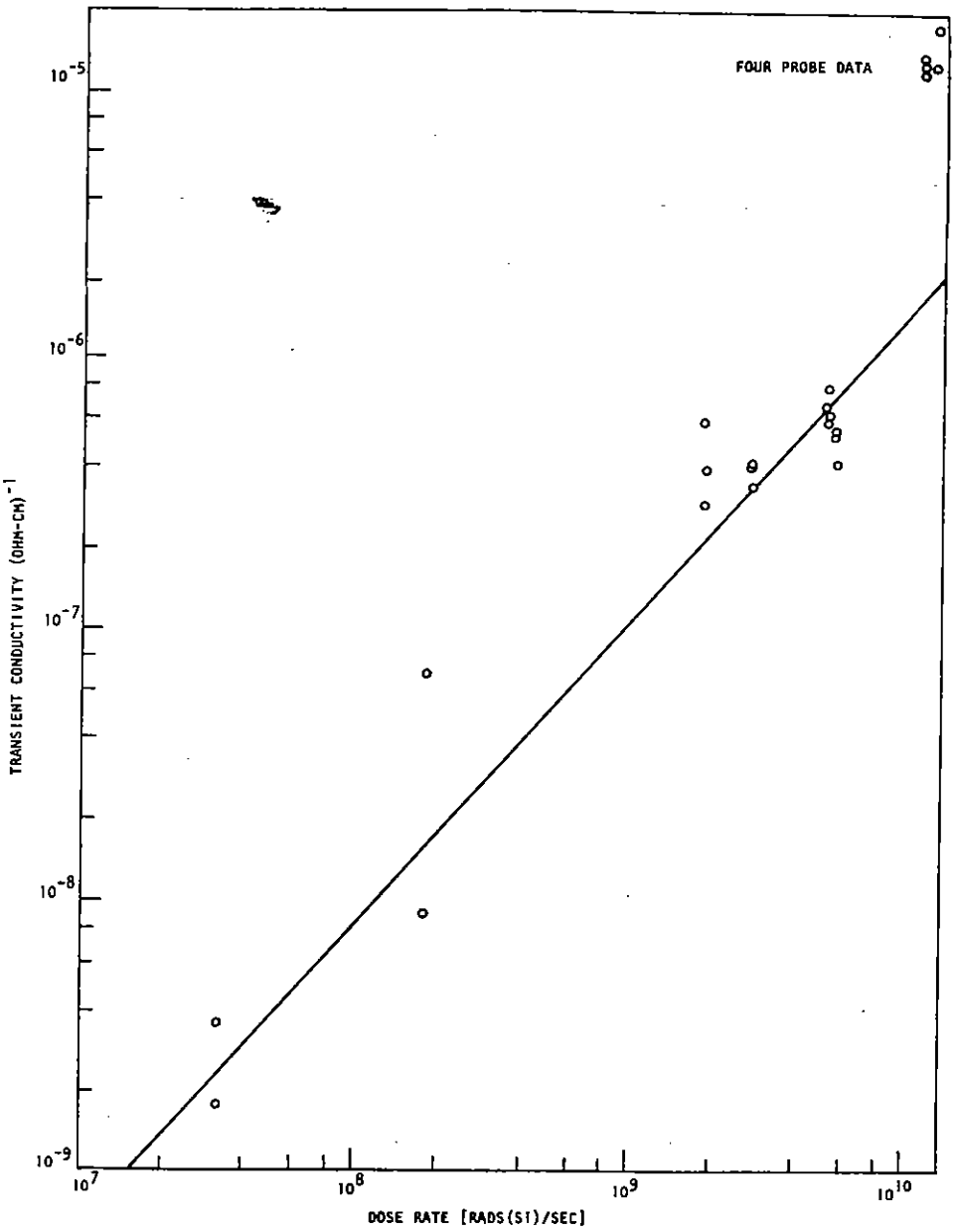

Fig. 24 Transient conductivity as a function of dose rate for wet sample (SS-1-2, SS-1-3) at 62°C. $\sigma_p = 1.0 \times 10^{-17} (\dot{\gamma})^{1.12}$.

Figure 25 shows a schematic of the four-probe experiment. The end pieces, A, A′, had silver contacts deposited over one side only, and performed the role of current injector and extractor, respectively. Sample S was a new piece of concrete, uncoated, sandwiched between A and A′. Potential probes in the form of fine platinum spirals were placed between the sample S and the electrodes A and A′. Under pressure, the interface containing the probes became very thin.

Polarization effects and space charge are assumed to affect only a shallow depth of the end pieces, and the current density at the position of the probes is expected to be uniform and given by the current entering the end pieces and the area of the probe interfaces. Since a very small current is drawn by the probes, only a very small, negligible amount of polarization or charge buildup will occur. Because the concrete is a relatively good conductor, no potential gradient can exist across the face of the sample. The major source of error in the measurement of the transient conductivity is in the definition of the irradiated area. Because it was not possible to uniformly irradiate the entire area of this particular sample, it was necessary to restrict the diffused beam with a large collimator and then calculate the effective area of the sample irradiated. This was done by placing a glass disc against the sample holder and coloring it brown with the Linac beam. The coloration was scanned with a densitometer, and the 50% points were taken as the effective area. Since the relative conductivity as a function of dose rate was sought, the estimation of the area is adequate for the experiment.

The computed transient conductivity for sample (S-1-4) in the saturated condition (5.5% water by weight) is included in Fig. 24, and places a lower limit to the transient conductivity of the wet concrete at 20°C. The data taken at lower dose rates were of the order of the noise (secondary emission effects) and were excluded from the figure. The computed resolution of the instrumentation used in the four-probe experiment was of the order of 10^{-6} $(\text{ohm-cm})^{-1}$. The important conclusion from the four-probe measurements was that the transient conductivity measured at lower dose rates was less than the value measured at $\sim 10^{10}$ rad/sec, and the roll-off of the data in some samples tested was an artifact of the electrode system and not a result of a peculiar conductivity mechanism.

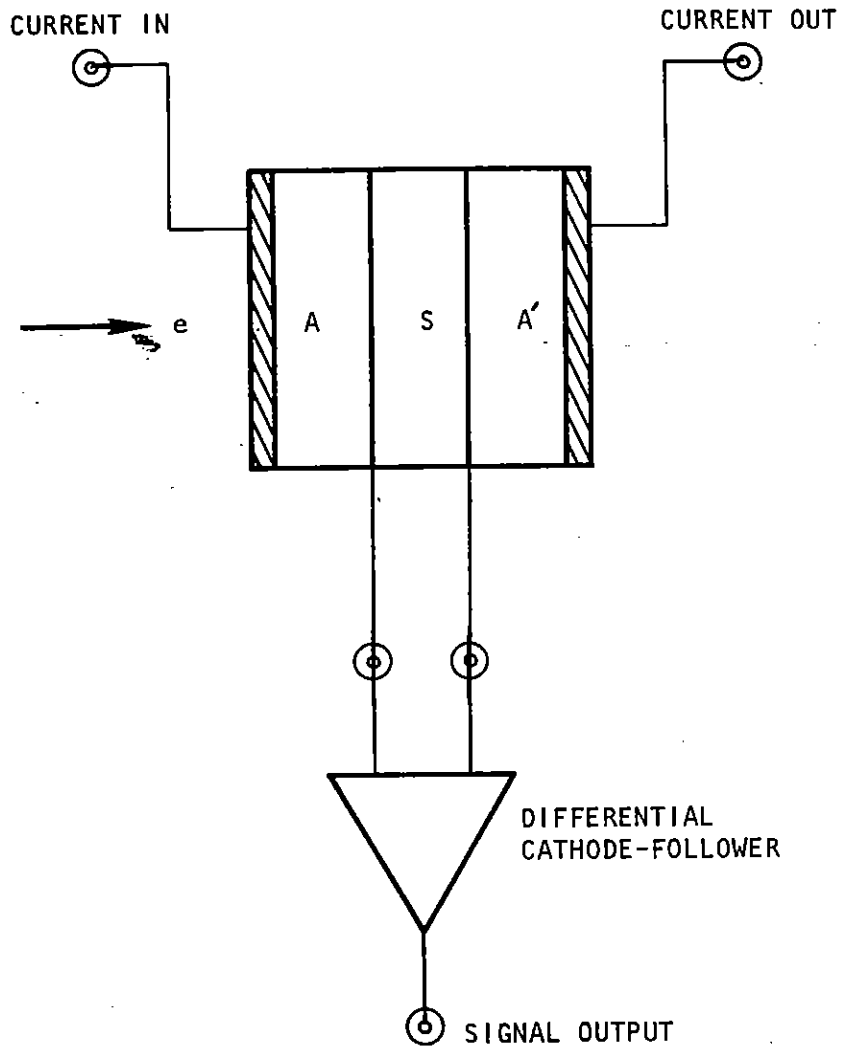

Fig. 25 Schematic of the four-probe conductivity experimental arrangement. Concrete Sample A,A have silver contacts on one side only; concrete sample S is uncoated and is the sample being measured.

5. SUMMARY AND DISCUSSION

The results of the tests are summarized in Tables 1 and 2. Table 1 is arranged so that the water content by percentage weight increases toward the bottom of the table. The water content is written in parentheses below each sample identification code. Where there are two numbers, the weight-percent of water was different for the two samples used in the measurement, and the percentage for each sample is given. The temperatures designated as "low," "room," and "high" correspond roughly to -50°, +20°, and +100°C, respectively. In general, it is seen that at a given temperature the water content largely determines the conductivity. The composition also influences the conductivity, as is seen by comparing the results of the saturated samples SS-1-2,3 and SS-1-4, which come from different positions on the same slug. The water content of SS-1-4 is a little higher, but the conductivity is higher than just the water content change would indicate.

The measurements on SS-1-4 were made using platinum Ag:AgCl blotter electrodes, and the results compare well with the measurement made with silver electrodes, considering the sample differences. The waveshapes observed with the two measuring techniques are very similar. The values of the ambient conductivity are somewhat lower than reported by the U.S.G.S.[7] for samples of concrete using ac measuring techniques. An ac measurement on SS-1-2,3 yielded the same value for conductivity as did the pulse technique, within experimental error.

The temperature dependences of wet samples do not follow the e^{aT} relation observed for water-bearing rocks, since a linear plot is not obtained when log σ is plotted versus T. This is probably because the e^{aT} dependence is essentially the dependence of the water in the pore volume[8] and does not account for increased ion concentration due to a temperature-dependent solubility of the materials in the concrete.

Since the wet samples are dominated by the water conductivity, and since this conductivity is almost certainly ionic, it is useful to obtain

Table 1

SUMMARY OF AMBIENT CONDUCTIVITY RESULTS

	Low Temp.	Room Temp.	High Temp.	$\sigma = \sigma_0 \exp(-E/kT)$
WE-1,2 (<0.1%) σ^*	2×10^{-9}	2.5×10^{-7}	3×10^{-6}	$0.15\ e^{-0.34/kT}$
S-1-2,3 (0.7%,1.2%) σ		2×10^{-6}		
WW-2-1 (1.2%) σ	1.1×10^{-8}	2.6×10^{-6}	4.0×10^{-5}	$11.5\ e^{-0.40/kT}$
SS-1-2,3 (1.2%,1.6%) σ		1.7×10^{-6}	1.0×10^{-4}	
S-2-1,3 (1.5%,1.6%) σ		3×10^{-6}		
SS-1-2,3 (5.7%,2.4%) σ		1×10^{-4}		
SS-1-4 (5.9%) σ	5×10^{-6}	2×10^{-4}	4.5×10^{-4}	

*σ is in $(\text{ohm-cm})^{-1}$

Table 2

SUMMARY OF TRANSIENT CONDUCTIVITY RESULTS

	Low Temp.	Room Temp.	High Temp.
WE-1,2 (0.01%)			
σ_0*	2.1×10^{-19}	3.4×10^{-19}	2.5×10^{-18}
Δ	1.2	1.2	1.2
S-1-2,3 (0.7%,1.2%)			
σ_0	1.1×10^{-14}	2.8×10^{-13}	1.1×10^{-14}
Δ	0.78	0.70	0.78
WW-2-1 (1.2%)			
σ_0	1.6×10^{-14}	2.2×10^{-15}	1.6×10^{-14}
Δ	0.62	0.86	0.74
SS-1-2,3 (1.2%,1.6%)			
σ_0	6.8×10^{-14}	5.6×10^{-15}	5.2×10^{-13}
Δ	0.66	0.80	0.66
S-2-1,3 (1.5%,2.4%)			
σ_0	2.8×10^{-14}	2.4×10^{-15}	2.8×10^{-14}
Δ	0.72	0.91	0.72
S-2-1,3 (4.6%,6.1%)			
σ_0	1.6×10^{-14}	1.2×10^{-12}	1.6×10^{-14}
Δ	0.82	0.65	0.75

*σ_0 in $(\text{ohm-cm})^{-1}$

an order-of-magnitude estimate of the average ion concentration. A fairly optimistic number for the mobility of ions in solution at room temperature is 10^{-3} cm^2/volt-sec.[2] Then, from Eq. 2,

$$N = \frac{\sigma}{e\mu} = \frac{2 \times 10^{-4}}{(1.6 \times 10^{-19})(10^{-3})} \approx 10^{18} \text{ cm}^{-3} , \qquad (8)$$

for wet samples, while $N \approx 10^{16}$ cm^{-3} for the ambient humidity samples.

Table 2 shows the transient results in a similar format to Table 1. The four-probe results and the sample SS-1-2,3 (wet) will be discussed separately.

The data are represented by the fitting parameters for

$$\sigma = \sigma_0 \dot{\gamma}^{\Delta} . \qquad (9)$$

The data fit an expression of this form within the accuracy of the experiment in most uses, and such a form appears to be a reasonable scaling law for the phenomena observed. This is to be expected in light of the considerations described in Section 2.

The three sets of samples, WW-2-1, SS-1-2,3(dry), and S-2-1,3, all show similar behavior. If we apply the model described in Section 2, we find that the temperature which characterizes the trap distribution is given by

$$T_1 = \frac{\Delta}{1 - \Delta} T . \qquad (10)$$

Averaging the results for these three samples, we find the results in Table 3.

Table 3

AVERAGE RESULTS FOR WW-2-1, SS-1-2,3, AND S-2-1,3

T(° K)	$\bar{\sigma}_0$	$\bar{\Delta}$	T_1(° K)
220	$4 \pm 2 \times 10^{-14}$	0.67 ± 0.03	447 ± 60
300	$3.4 \pm 1.5 \times 10^{-15}$	0.86 ± 0.03	1840 ± 460
370	$2 \pm 1.8 \times 10^{-13}$	0.71 ± 0.03	1520 ± 220

Within the spread of values of Δ, the 300°K and 370°K temperatures cannot be definitely said to be different. This indicates that the distribution of traps in energy remains about the same above between about 0°C and 100°C. If anything, the traps move slightly closer to the energy of the free states. The low characteristic temperature for the -50°C data indicates that the trap distribution has shifted considerably toward the free states, probably due to freezing of the liquid and to thermal contractions of the concrete matrix.

The factor σ_0 reflects the mobility, the density of free states to which the electrons can be excited, the trap density, and the capture rate of the immobile states. A decrease of the mobility can account for the decrease in σ_0 between -50°C and 0°C, while a decrease in the trap density with liquid melting could account for the large increase in σ_0 above 0°C. This is consistent with the change in Δ, since a decrease in the density of shallow trapping states would increase T_1 (move the center of the trapping distribution deeper in energy) and increase σ_0.

Thus, the values in Table 3 appear to represent some reasonable behavior in concrete samples with ambient water content (1.2% and 2.4% by weight), and we may write

$$\sigma_{TOT} = 11.5\, e^{-0.40/kT} + \sigma_0 \dot{\gamma}^{\Delta} \quad , \tag{11}$$

where σ_{TOT} = ambient plus RIC and the values of σ_0 and Δ are taken from Table 3.

The vacuum-dry sample WE-1-2 cannot be analyzed using the model described in Section 2, since $\Delta > 1$. Rose[6] does describe a model which predicts superlinear dependence on the generation rate, involving two types of traps separated in energy. The argument depends on detailed trap-level structure; since we can only speculate at this stage about the level structure in vacuum-dry concrete, and since this sample was run for comparison rather than for applicable data, we will not go into details on the model. We mention it to point out that a $\dot{\gamma}^{1.2}$ dependence is not out of the question, and that similar superlinear dependences have been seen in other materials.

The fact that S-1-2,3 (0.7%, 1.2%) behaves more like S-2-1,3 (4.6%, 6.1%) than like the other samples with water contents in the 1% to 2% range is a bit puzzling. However, S-1-2,3 has a large chunk of aggregate which occupies about half of the sample electrode area, while in the other samples, the aggregate was in smaller chunks in the region of the electrodes. We do not understand the mechanism for the RIC changes observed, but we feel that the size of the aggregate in S-1-2,3 makes it less representative of an average value for the 1 to 2% water content range than the other three samples examined in this range.

For the wet (saturated) sample S-2-1,3, the characteristic temperatures associated with the trapping levels are given in Table 4.

Table 4

CHARACTERISTIC TEMPERATURE FOR S-2-1,3 (WET)

T°K	Δ	T_1(°K)
220	0.75	660
293	0.65	540
352	0.82	1600

The characteristic temperature at the high temperature is seen to be about equal to that for the 1 to 2% water content samples, but the shift in the trapping level distribution apparently occurs at a higher temperature in the saturated sample. The changes in σ_0 with temperature are difficult to explain since the same mechanisms should be taking place in both the ambient and saturated samples. The larger average ion concentration in the wet samples will result in a reduced mobility above the freezing points, and this may be responsible for this behavior.

The divergence of behavior between S-2-1,3 (wet) and SS-1-2,3 (wet) is even more difficult to explain, especially since SS-1-2,3 (ambient) behaved reasonably compared to WW-2-1 and S-3-1,3 (ambient). There are indications that the sublinear behavior of the RIC in SS-1-2,3 (wet) at high dose rates is an experimental artifact. The first indication is that, since the sample was first run in the ambient moisture condition and later in the saturated condition, some degradation of the electrodes is expected. We found that

the silver-deposited electrodes on wet samples showed increasing polarization effects with time, and the polarization becomes severe after the sample has been saturated for a week or so. SS-1-2,3 (wet) could then be expected to show successively stronger polarization effects when larger currents were passed through it. This could account for the odd behavior of this sample.

Also, a saturated sample run with the four-probe technique did not exhibit roll-over, nor did S-2-1,3 (wet), which seemed to confirm our suggestion that this was an experimental artifact induced by degraded electrodes.

Even if the strange behavior should be real, the RIC in SS-1-2,3 (wet) is below S-2-1,3 (wet) at high dose rates and, therefore, the latter sample constitutes the "worst case" among the wet samples tested. Note that the four-probe measurements agree with the results of S-2-1,3 (wet).

An expression for the total conductivity of the wet samples cannot be written in the straightforward way of Eq. 11, since the ambient conductivity cannot be described by a single activation energy over the temperature range of interest. However, we can write

$$\sigma_{TOT} = \begin{Bmatrix} 4 \times 10^{-4} + 1.6 \times 10^{-14}\, \dot{\gamma}^{0.75} & T \sim 100^{\circ}C \\ 2 \times 10^{-4} + 1.2 \times 10^{-12}\, \dot{\gamma}^{0.65} & T \sim 20^{\circ}C \\ 2 \times 10^{-6} + 1.6 \times 10^{-14}\, \dot{\gamma}^{0.82} & T \sim -50^{\circ}C \end{Bmatrix} . \quad (12)$$

Equations 11 and 12 present averages over the samples for which the data appear to best represent the concrete material. Extrapolations of these scaling expressions to higher dose rates are shown in Fig. 26 for ambient humidity samples and in Fig. 27 for saturated samples. Also indicated are representative values of the ambient conductivity for these two types of samples.

Let us now consider, as best we can from the limited number of samples available, the magnitude of the deviations from the average curves in Figs. 26 and 27. The deviation in σ can be written

$$\frac{d\sigma}{\sigma} \approx \frac{d\sigma_0}{\sigma_0} + d\Delta \log \dot{\gamma} \quad . \quad (13)$$

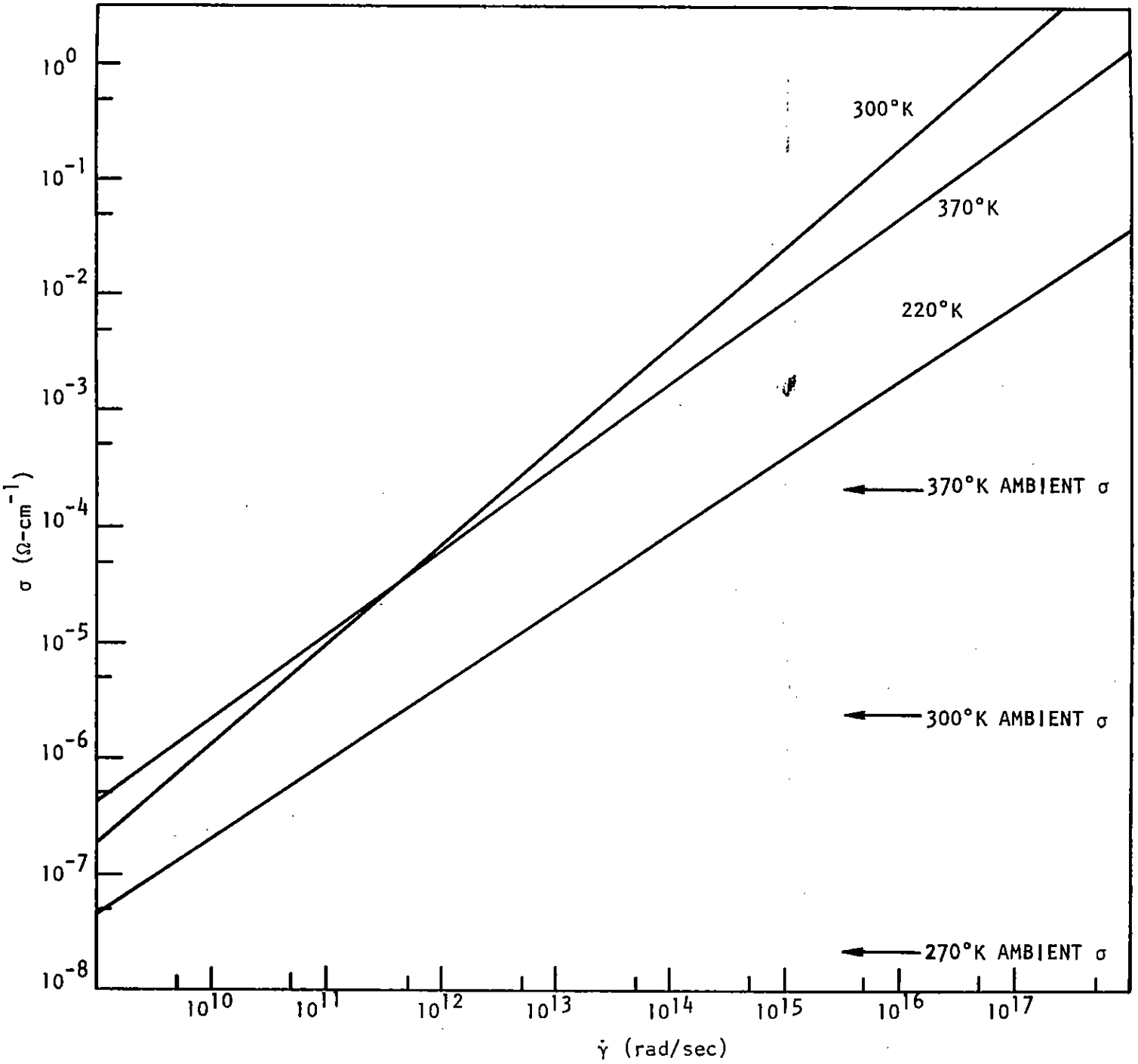

Fig. 26 Conductivity in concrete sample with 1-2% water content by weight

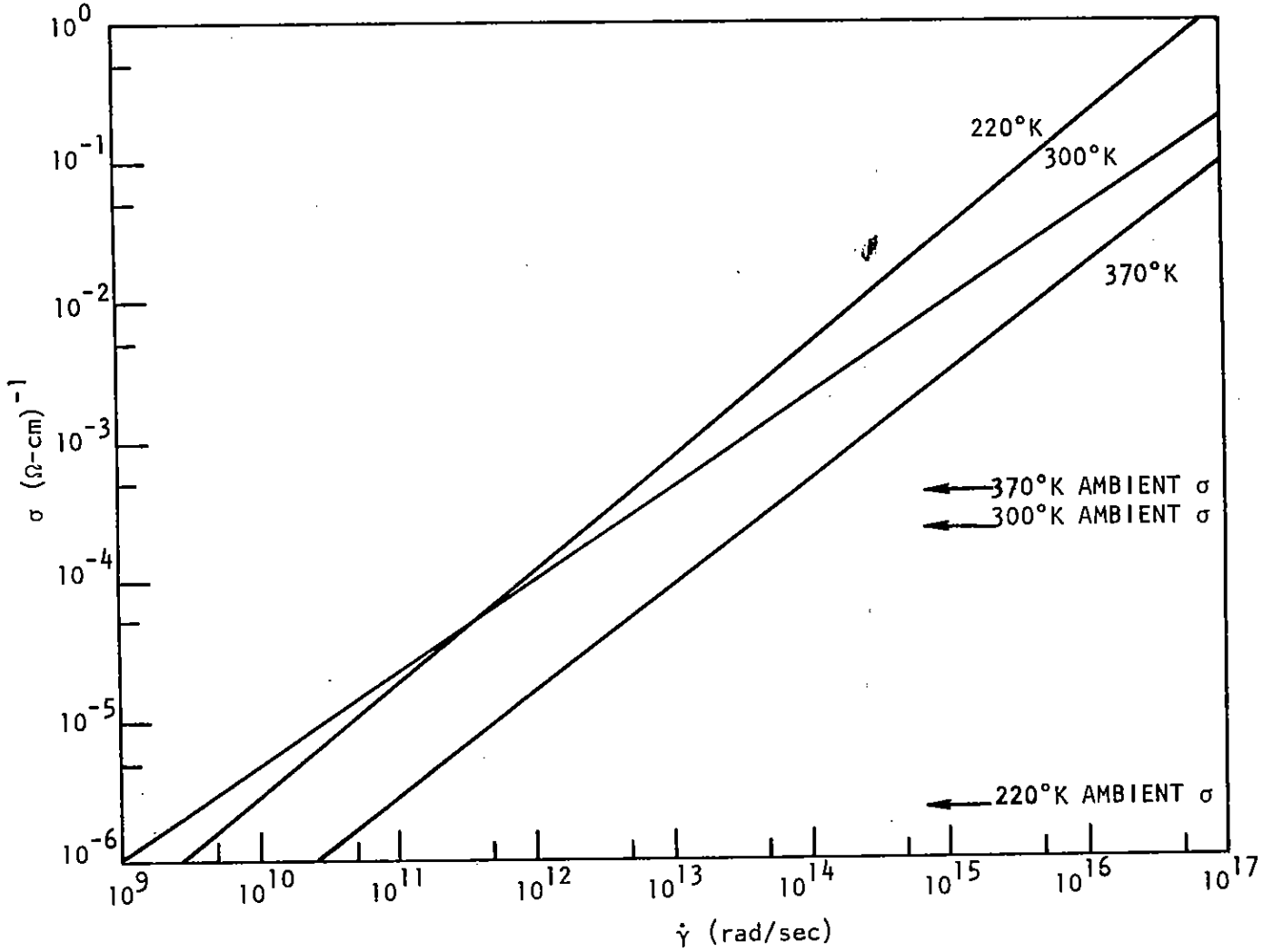

Fig. 27 Conductivity in saturated samples

Considering average deviations, the spread in σ_0 was found to be ~100% for a given type of sample at a given temperature, while the average in Δ was ~5%. Thus, at 10^{16} rad/sec, on the average

$$\frac{d\sigma}{\sigma} \approx 1 + 0.5\,(16) \approx 2 \quad .$$

As a worst case, $d\sigma_0/\sigma_0 \approx 10$ and $d\Delta \approx 0.2$ and

$$\frac{d\sigma}{\sigma} \approx 10 + 0.2\,(16) \approx 13 \quad ,$$

or a little over an order of magnitude. The actual uncertainty is certainly less than the worst case, since the conductivity in a given structure will be the average of the conductivity of small volumes. Since most of the volume of the concrete tested in these experiments behaved like the average plots in Figs. 26 and 27, the average over a reasonable volume of a structure should be within a factor of 5 of the average at 10^{16} rad/sec.

Another source of uncertainty is introduced by the decrease in mobility at high dose rates due to the increased ion concentration. We can estimate this as follows. The increase in ion concentration is approximately equal to the electron concentration

$$n \propto \dot{\gamma}^{\Delta} \quad . \tag{14}$$

at 10^9 rad/sec, we estimated in Section 2 that $\tau_e \leq 10^{-9}$ sec and $g \approx 10^{21}$ $(cm^3\text{-sec})^{-1}$, which yields $n \leq 10^{12}$ cm^{-3}. At 10^{16} rad/sec, taking $\Delta \approx 0.8$, $n \leq 10^{16}$ cm^{-3}. Since the ion concentration in the ambient samples without radiation is 10^{16} cm^{-3}, the added ions will decrease the RIC by, at most, a factor of 2 due to mobility changes, and will not affect the wet samples significantly. Since τ_e is probably much less than 10^{-9} sec at 10^9 rad/sec, the decrease in mobility is probably not important.

If further refinement of these results is required, the most fruitful approach seems to be to establish a correlation between the RIC and parameters of the material such as porosity, ratios of aggregate volume to concrete volume, and perhaps ratios of aggregate surface to aggregate volume.

This could be accomplished by sampling the RIC of small areas of concrete samples by collimating the electron beam to a small spot and correlating the results with small area structure, or by making concrete samples under controlled conditions.

6. CONSIDERATION OF OTHER SITE MATERIALS

The feature of the nonstructured site material, such as earth and fill materials, which makes that material so difficult to characterize, is the variability in the relative composition of air, solid material, and water. The proportion of these components in a sample of material will vary greatly with position, depth, and history. As has been seen, the pore water exhibits a sublinear dependence on dose rate, and air conductivity has been found to be approximately linear in the dose rate, and the RIC in the solid matrix can have a sublinear or a superlinear dependence on dose rate. Thus, the RIC in the site materials can differ by orders of magnitude for different places in the site.

The brute force solution to the predictability problem is to homogenize the site materials and fix the water content, and this may be possible in future site construction. This will add considerably to the cost of the site, and a more efficacious way to approach the problem is to correlate the RIC with composition and then work for a composition which minimizes the problem in critical areas.

In the absence of interface effects, the conductivities of each of the components of the porous mixture should add; i.e.,

$$\sigma = \frac{1}{V} \sum_i V_i \sigma_i \ ,$$

where V = total sample volume being considered,

σ_i = conductivity of i^{th} component,

V_i = the part of the sample volume occupied by the i^{th} component.

The absence of interface effects implies that the transport of carriers is not limited by the barriers formed by junctions between two materials. If such a limitation exists, charge accumulation at interfaces makes the problem nonlinear.

There are at least two indications that charge accumulation at interfaces may not be significant. The first is that a salt solution is known

to be one of the best electrical contacts for insulation conductivity work. The second is that no space-charge buildup was observed in the experiments on concrete. Thus, the superposition of the conductivities appears to be a reasonable model to start with. The model can be verified by measuring the RIC as a function of relative proportion of one component—say, water —for several different surface-to-volume ratios in the solid matrix. Interface effects, if present, should be revealed in the results.

If the results indicated that the structure, as well as the composition, is significant, the above expression for the conductivity should be modified by multiplying by a function of the surface-to-volume ratio. This function can be experimentally determined.

Correlation experiments can then be run to determine RIC in

1. the gravelly clay as a function of density for at least two water contents,
2. the gravelly clay as a function of water content,
3. the pore or ground water,
4. moist cracked rock.

Each of these should be measured at several temperatures.

The results of these experiments can be used to predict a worst-case enhancement, and the conditions of minimum enhancement. Samples from the site should then be selected which match as closely as possible the worst case and the best case; these samples should be carefully transported to a test facility, and the RIC measured to verify the predictions.

Following the above plan will result in no better than order-of-magnitude confidence in a prediction of the average RIC in a cable-run size portion of a site due to the variability of composition and meteorological conditions. However, as long as we are dealing with mixtures of natural earth and unknown water and temperature conditions, we do not see that more extensive tests would improve the confidence of the predictions. In our opinion, greater accuracy can be achieved only by exerting some control over the site material itself.

6.1 PORE AND GROUND WATER

The evaluation of the conductance properties of ground water is expected to be the single most important step in the program. The reasons are that the water conductance will be the greatest part of the total conductance, and that the electrode system must be found suitable for reversible, or satisfactory, ion exchange with the ions in the water before proceeding.

Suitable working electrodes should be chosen which will produce minimum polarization and chemical action at the electrode-sample interface. The most attractive electrode system and the one that will be evaluated first is the metal:metal sulfate such as $Pb:PbSO_4$. The sample holder for the liquid will be of simple glass construction, using the guarded electrode structure and a four-probe measurement. Water from the ground at the site should be used.

The RIC of ground water will be determined versus dose rate and temperature, and then the program will continue to the soil-water measurements.

6.2 SOIL

The typical soil of concern to the program is a silty-gravelly clay found within the first foot of depth at the site. Not more than three representative samples of soil should provide a sufficient characterization of the RIC if the water content is adjusted properly. The water content should be varied between the saturated condition and the ambient, while the density of the samples should closely resemble that of the undisturbed site composition. The effect of perturbations on the density should be examined. These conditions should scope the worst case.

6.3 CRUSHED ROCK

The conductance of the crushed rock will be dependent on the degree of moisture present: a completely saturated rock conductance will be given by the water conductance. The conductance of the wet case will be a sum of the humid air (pore) conductance and the conductance of the water film on the rock surface; the conductance of the dry case will be given by the pore

air conductance. In all cases, the rock conductance is expected to be dominated by the water conductance and the air conductance.

The saturated and dry situations are considered cases of either water or air conductance, and can be scoped by considering the effective area or the volume available for conduction. The intermediate case is more difficult to evaluate and will require the measurement of a sample with known moisture content.

6.4 TEMPERATURE EFFECTS

The effects of temperature variations on the conductance of composite samples will be considered as the separate systems are evaluated. Due to the uncertainties expected to arise from the ice-water and water-air mixtures, the temperature dependence will be examined for the worst case during the soil measurements. The phase change expected in freezing water and its bulk or pressure effects preclude measurements of the temperature dependence in ground water. Also, the severe temperature dependence of the moisture content of air, in the crushed rock case, is expected to introduce more uncertainties. However, since the mobility of ions is greatly reduced in wet air, the worst case is expected to be just above the freezing point of the water.

6.5 CONCLUSIONS FROM THE STUDY OF NONSTRUCTURAL MATERIALS

Tests can be performed which will allow worst-case predictions and identify ways to minimize the RIC in site materials. Only order-of-magnitude predictions can be expected from such tests due to the uncertainties in (1) local variations in material and weather conditions and (2) disturbance of the test samples in collecting and transporting. Such tests can be carried out as a logical extension of the concrete experiments, with some modification of the equipment.

More accuracy can be obtained if controlled fill materials are used, since they can be tailored for minimum response and samples can be prepared in the laboratory.

As a final note, it may well be more economical to fill critical areas with an inherently low RIC material than to attempt to accurately characterize existing site materials.

Appendix

ELECTRODE STUDIES

The original choice of silver to be used as the electrode material was made over other metals, such as gold, platinum, and aluminum, primarily because of the following considerations.

1. Silver is easily evaporated and deposited.
2. Electrodes could take a solder easily, if necessary.
3. Chemical effects on the film would produce a conductive, easily reversible intermediate compound.
4. Platinum would result in large polarization effects if current was drawn; gold was expected to behave in a similar manner.
5. Aluminum oxidizes easily to form an insulating layer of oxide.

The predicted compounds of silver formed by contact with the water contained in concrete were primarily AgOH and AgCl because it was assumed that the CL^- and OH^- ions were found in high concentrations in the pore water.

Because the measurements of the transient conductivity in concrete were producing results which were puzzling and could not be interpreted by previous radiation effects experience, a mechanism which would explain the effects was sought in the electrode system. Some experiments were planned to measure the ambient conductivity of a sample of concrete with an accepted electrode system and then to make a comparison of the conductivity measured by using the conventional silver electrodes.

Through the courtesy of Mr. Robert Bigelow of the USGS, a set of reversible Ag:AgCl electrodes was obtained which consisted of two sheet brass discs ~2-1/4 in. in diameter, treated in such a way as to have the active faces coated with a layer of platinum black (essentially a platinum colloid); also, four absorbent paper circles or "blotters" prepared by treating a special blotter paper with various reagents, so that a suspension of colloidal silver and silver chloride remained in the paper.

In the experiment, a clean sample of saturated concrete was sandwiched between, respectively, the blotters, the platinum black electrodes, a cushion of glass filter paper, Pyrex discs, and a weight to hold the assembly together under pressure. The assembly was contained in a large straight-wall Pyrex dish. Distilled water was added until the entire assembly, between the platinum electrodes, was submerged. After a period of time, sufficient for equilibrium to be established, the water was drawn off and measurements were made. The applied voltage was either a positive or a negative pulse with a duration of ~350 μsec; no attempt was made to depolarize between measurements, although the efficacy of depolarization was checked. The current passed by the assembly was measured by the voltage drop across a selectable load resistor. Both signals were displayed on a dual-trace Tektronix Type 556 oscilloscope. Although not necessary, photographs were taken to facilitate the measurements. No change in the signal amplitudes was seen using either single pulses with polarity reversal or continuous monopolar pulses at ~120 pulses per sec.

The conductivity of the sample was calculated knowing its thickness, area, the current passed, and the voltage across the electrodes.

Next, the sample was removed and quickly dried, and silver contacts over both faces were applied by evaporation. The sample was reevacuated and then saturated with water in the usual way. It was assembled in the same way as the blotter experiment except that silver wires were pressed against the electrodes for current leads. Measurements were taken, and the conductivity was calculated over several days.

The measured conductivities are shown in Table A1.

Table A1

COMPARISON OF ELECTRODES

	(Ambient Conductivity $(ohm\text{-}cm)^{-1}$)					
	Initial		After 1 Day		2 Days	3 Days
Electrode	Ag:AgCl	Ag	Ag:AgCl	Ag	Ag	Ag
WE-1-2	3.6×10^{-4}		3.8×10^{-4}			
N-2-3	2.4×10^{-4}	3.0×10^{-4}		1.8×10^{-4}	1.8×10^{-4}	1.6×10^{-4}

The variation in the conductivity of the control sample and in the experimental sample using the two-electrode systems can be explained by the sample temperature variations between the measurement periods. However, the obvious decrease in the measured conductivity using the silver electrodes must be construed to be a degradation due to chemical changes in the silver-concrete interface.

It may be noted at this point that during the course of these experiments, the discovery was made that both the Ag:concrete and the Ag:AgCl:concrete systems store electro-chemical energy. After several hundred 100-mA pulses, ~350 μsec wide, were applied to the sample, a voltage could be measured across the electrodes and a momentary current of up to ~0.75 mA could be drawn. The decay of the current was found to be exponential with a decay of ~2 to 4 sec, using a 1-ohm load.

A further observation was made, during the measurements using the Ag:AgCl electrodes, that there appeared a charging current and decay, indicating polarization effects, similar to those observed in the Ag:concrete system. To check the quality of the electrodes, a dummy sample was made from a stack 1 cm thick of 3-cm-diameter glass filter paper, and placed between a set of clean Ag:AgCl electrodes. The assembly was soaked with 0.01 N NaCl solution. No quantitative measurements were made, but the voltage and current characteristics were carefully examined for charging or polarization effects. None was observed, and no battery effect was observed.

Typical oscilloscope pictures are shown in Fig. A1. Figure A1(a), upper trace, is the voltage applied across the Ag:AgCl electrodes placed against a stack of glass filter-paper discs saturated with 0.01 N NaCl solution. The lower trace in the voltage developed across a 1-ohm resistor and is a function of the current flowing through the stack. There is no evidence of polarization or deterioration. Pulse length is 350 μsec.

Figure A1(b), upper, shows the voltage across the Ag:AgCl blotter electrodes placed against a wet sample (N-2-3) of concrete. The lower trace represents the current flowing through the sample and shows a little polarization. Figure A1(c), lower, represents the current flowing through N-2-3 after it had been coated with silver. The trace indicates polarization, but the degree of polarization is about the same as in (b).

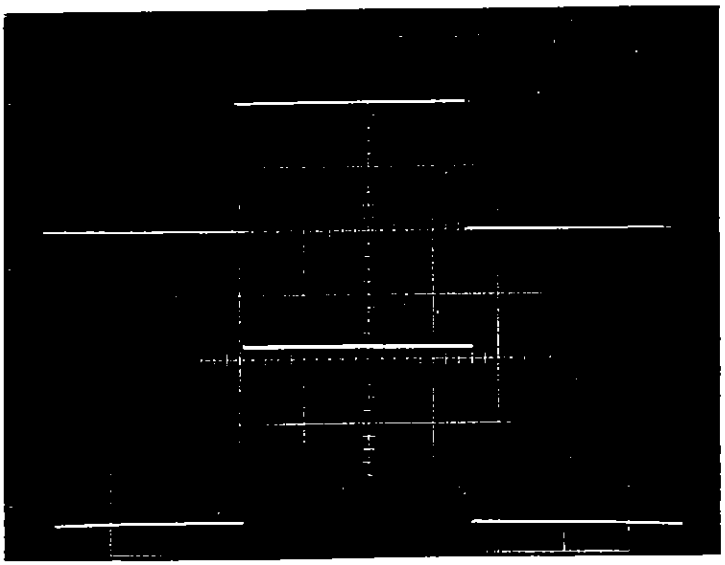

(a)
Upper Trace
Applied Voltage: 10 V/cm
Lower Trace
Current Pulse: 0.2 amps/cm
Sweep: 100 μsec/cm

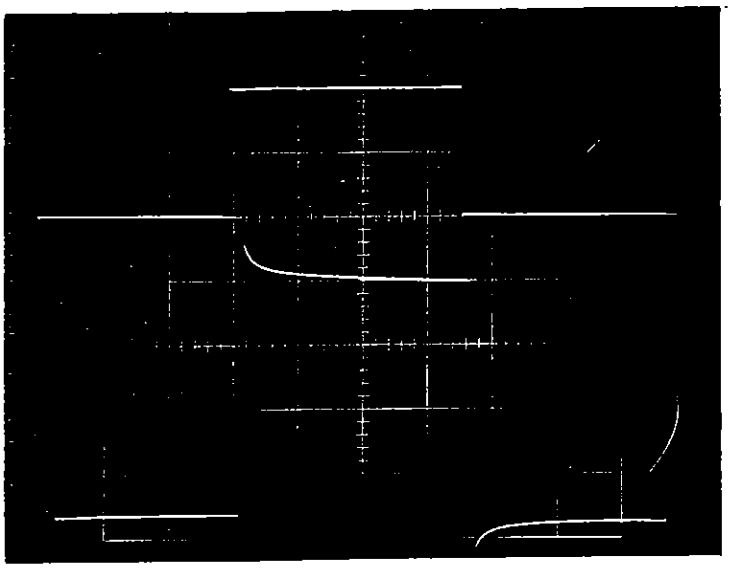

(b)
Upper Trace
Applied Voltage: 10 V/cm
Lower Trace
Current Pulse: 5 mA/cm
Sweep: 100 μsec/cm

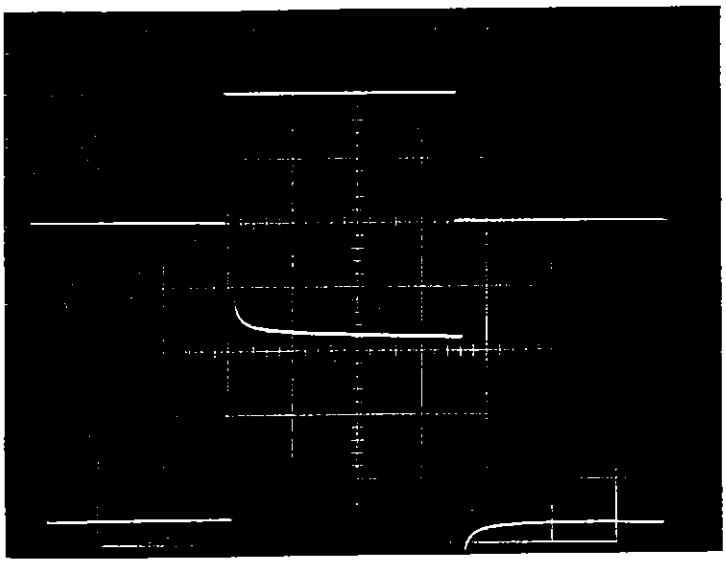

(c)
Upper Trace
Applied Voltage: 10 V/cm
Lower Trace
Current Pulse: 2 mA/cm
Sweep: 100 μsec/cm

Fig. A1 Typical oscilloscope photographs (a) Ag:AgCl:filter paper:0.01 N NaCl; (b) Ag:AgCl:concrete; (c) Ag:concrete

In order to understand the behavior of the Ag:AgCl:concrete and the Ag:concrete systems, some electrochemical experiments were performed using silver wire and silver film deposited on glass microscope slides, and using both 0.01 N NaCl solution and distilled water for the electrolytes.

The ions assumed most likely to contribute to the conduction process in concrete are H^+, OH^-, Cl^-, and Na^+. Possible reactions at the silver electrodes, in a 0.01 N NaCl solution, are

	$Na^+ + e \rightarrow Na$	(1)
Cathode	$2H_2O + 2e \rightarrow H_2 + 2\ OH^-$	(2)
	$2\ H^+ + 2e \rightarrow H_2$	(3)
	$AgCl + e \rightarrow Ag + Cl^-$	(4)
	$AgOH + e \rightarrow Ag + OH^-$	(5)
	$4\ OH^- \rightarrow 2\ H_2O + O_2 + 4\ e$	(6)
Anode	$2\ Cl^- \rightarrow Cl_2 + 2\ e$	(7)
	$Ag + Cl^- \rightarrow AgCl + e$	(8)
	$Ag \rightarrow Ag^+ + e$	(9)
	$2\ Ag + 2\ OH^- \rightarrow Ag_2O + H_2O + 2\ e$	(10)
	$2\ Ag + 4\ OH^- \rightarrow AgO\ (\text{or}\ Ag_2O_2) + 2\ H_2O + 2\ e$	(11)

Observations of the reactions occurring at the electrodes while a direct current is passing through the cell, such as the formation of a precipitate or a coating or gas bubbles, are:

(Reactions 1, 3, 6, and 7 are not observed for energetic reasons.)

a. The cathode surface remains bright and metallic and produces a gas so (2) is predicted; (4) might occur momentarily if a thin layer of chloride is formed prior to electrolysis.

b. At a low current density, no gas is given off at the anode while it is seen to turn white and produce a fine white precipitate. Therefore, (6) and (7) are eliminated, (8) is predicted, (9) is difficult but would appear as (8) if it did occur.

In distilled water, no white coating or precipitate is seen on either the anode or the cathode; instead, a brownish-black coating forms on the anode. The most probable reactions are, thus, (10) and (11).

Examination of areas on irradiated concrete samples, whose silver coating had adhered to the polyethylene and had been pulled off, shows a black stain resembling Ag_2S or AgO in color rather than the brown Ag_2O.

The possibility that the coating is a sulfide requires that the following reaction take place:

$$2\ Ag^{+} + S^{=} \rightarrow Ag_2S \quad .$$

The estimated SO_3 concentration in both Type 1 and Type 2 Portland cements[A1] is between 1.9% and 2.7% by weight and in concrete appears as the sulfate. In a wet concrete, therefore, the sulfate ion concentration is expected to be relatively high, and during radiolysis it is conceivable that

$$n\ (SO_4^{=}) \rightarrow nS^{=} + 4\ n\ [O]^{m} \quad ,$$

where the values of n and m are not known.

However, this reaction requires essentially a reduction, which is unlikely in an oxidizing situation such as exists during the radiolysis.

A reaction which is more likely in such an environment is the oxidation of silver to a higher valence state:

$$Ag^{+} \text{ to } Ag^{++} \quad ,$$

resulting in

$$Ag^{++} + O^{=} \rightarrow AgO \quad .$$

A consideration of the high sulfate concentration also provides a possible explanation of the battery effect observed in both electrode systems. The reaction

$$2\ Ag + HSO_4^{-} \rightleftarrows Ag_2SO_4 + H^{+} + e$$

is expected to be reversible and accounts for the effect. The experimentally observed potential of ~0.7 volt compares reasonably well to the electrochemical potential of the $Ag:Ag_2SO_4$ system of 0.799 volt.[A2] In addition, the insoluble Ag_2SO_4 formed would result in a decrease in electrode efficiency by decreasing the effective conductive area.

DISCUSSION AND CONCLUSIONS

Inspection of the Ag:AgCl blotter electrodes revealed that the areas of the blotters which were in contact with the porous areas of the concrete and where the current density was the highest were darkened, while those areas in contact with the low conductivity aggregate were still white. Also, the corresponding high-current areas on the concrete showed darkening due, most likely, to Ag^+ ions transferred to, and reduced on, the concrete.

Although no deterioration was observed in the performance of the Ag:AgCl electrode system over the period of these experiments, polarization effects were observed due to the small concentration of Cl^- in the concrete pore water. The success of these electrodes seems to be a result of their large effective area rather than of their reversibility. Based on these experiments, the known photosensitivity of AgCl, and the reactive species expected to be formed in the pore water in concrete during irradiation, it is concluded that for purposes of the determination of the transient conductivity in concrete, the Ag:AgCl electrode system offers little advantage over the pure Ag electrodes, as long as the Ag electrodes are fresh. For experiments lasting several days, the Ag electrodes degrade, and the Ag:AgCl system is preferred.

The results of workers in the electrochemical field on the silver-silver oxide reference electrode are interesting and could explain some of the anomalous behavior observed.[A3] The $Ag:Ag_2O$ reference electrode has been known for many years, but relatively little success has been realized in developing a system with a stable electrode potential. Soon after a freshly prepared electrode is immersed in the cell electrolyte, the potential begins to decrease slowly. The reason for the erratic behavior of the electrode potential appears to be the formation of a non-stoichiometric oxide layer by adsorption of oxygen from the electrolyte. This layer appears to be extremely subject to passivation. This is adequate to explain the partially reversible characteristics of the silver electrodes and, in addition, could explain the high apparent dose-rate dependence of the slope

on the conductivity of wet samples at low dose rates with the degraded electrodes. However, the effects of radiolysis on the stability of an established passivated layer are not known, and we can only speculate as to the mechanism responsible for the degradation.

The conclusions reached on the electrode and electrolysis experiments are that the silver electrode-on-concrete system suffers a gradual deterioration by chemical means, which is diffusion-limited. The rate is accelerated by high temperatures and, very likely, by the reactive species formed during irradiation. The deterioration comes about by a buildup of an insulating layer of silver oxide and silver sulfate in the interface, resulting in a decrease in the effective area of the electrode and a consequent localized increase in the current density.

Charge storage effects are observed, such as space charge and polarization, which are ion-concentration-dependent and result in a transient decrease in the internal field and, thus, the current through the sample. They are strongly dependent on temperature and water content.

REFERENCES

1. A. Rose, Concepts in Photoconductivity, Interscience, N.Y. 1963, p. 4.

2. Radiation Chemistry, J. Dobo and P. Hedvig, ed., Akademiai Kiako, Budapest 1967.

3. D. K. Nichols and V. A. J. van Lint, IEEE Trans. Nucl. Sci. NS-13, 119 (1966).

4. A. Rose, op. cit. p. 38.

5. V. A. J. van Lint, J. W. Harrity, and T. M. Flanagan, IEEE Trans. Nucl. Sci. NS-15, 194 (1968).

6. A. Rose, op. cit. p. 48.

7. R. Bigelow, private communication.

8. G. V. Keller in Handbook of Physical Constants, S. P. Clark, Jr., ed., Geological Society of America, 1966, p. 555.

A1. "Soil and Slope Stabilization and Moisture and Density Determination Developments," National Academy of Sciences National Research Council, Highway Research Board Bulletin 309, p. 59.

A2. Reference Electrodes Theory and Practice, D. J. G. Ives and G. J. Janz editors, Academic Press, New York (1961), p. 393.

A3. D. J. G. Ives, op. cit. p. 334.